Unleashing the Frequency: Multi-Megawatt Demonstration of 100% Renewable Power Systems with Decentralized Communication-Less Control Scheme

Przemyslaw Koralewicz, Emanuel Mendiola, Robb Wallen, Vahan Gevorgian, and Daniel Laird

National Renewable Energy Laboratory

NREL is a national laboratory of the U.S. Department of Energy
Office of Energy Efficiency & Renewable Energy
Operated by the Alliance for Sustainable Energy, LLC

This report is available at no cost from the National Renewable Energy Laboratory (NREL) at www.nrel.gov/publications.

Contract No. DE-AC36-08GO28308

Technical Report
NREL/TP-5000-80742
September 2022

Unleashing the Frequency: Multi-Megawatt Demonstration of 100% Renewable Power Systems with Decentralized Communication-Less Control Scheme

Przemyslaw Koralewicz, Emanuel Mendiola, Robb Wallen, Vahan Gevorgian, Daniel Laird

National Renewable Energy Laboratory

Suggested Citation
Koralewicz, Przemyslaw, Emanuel Mendiola, Robb Wallen, Vahan Gevorgian, and Daniel Laird. *Unleashing the Frequency: Multi-Megawatt Demonstration of 100% Renewable Power Systems with Decentralized Communication-Less Control Scheme*. Golden, CO: National Renewable Energy Laboratory. NREL/TP-5000-80742. https://www.nrel.gov/docs/fy22osti/80742.

NREL is a national laboratory of the U.S. Department of Energy
Office of Energy Efficiency & Renewable Energy
Operated by the Alliance for Sustainable Energy, LLC

This report is available at no cost from the National Renewable Energy Laboratory (NREL) at www.nrel.gov/publications.

Contract No. DE-AC36-08GO28308

Technical Report
NREL/TP-5000-80742
September 2022

National Renewable Energy Laboratory
15013 Denver West Parkway
Golden, CO 80401
303-275-3000 • www.nrel.gov

NOTICE

This work was authored by the National Renewable Energy Laboratory, operated by Alliance for Sustainable Energy, LLC, for the U.S. Department of Energy (DOE) under Contract No. DE-AC36-08GO28308. This work was supported by the Laboratory Directed Research and Development (LDRD) Program at NREL. The views expressed herein do not necessarily represent the views of the DOE or the U.S. Government.

List of Acronyms

AC	alternating current
ARIES	Advanced Research on Integrated Energy Systems
BESS	battery energy storage system
BMS	battery management system
DER	distributed energy resources
DOE	Department of Energy
ESS	energy storage systems
HVAC	heating, ventilation, and air conditioning
Hz	hertz
kV	kilovolt
kW	kilowatt
IBG	inverter-based generation
IBRs	inverter-based resources
MW	megawatt
MWh	megawatt-hour
MVA	megavolt-ampere
NREL	National Renewable Energy Laboratory
PV	photovoltaic
RoCoF	rate of change of frequency
RTAC	real-time automation controller
RTDS	real-time digital simulator
SCADA	supervisory control and data acquisition
SOC	state of charge
UFLS	under-frequency load shedding
UPS	uninterruptible power supply
VAR	volt-amps reactive

Abstract

Power systems, which range in size from small microgrids to island systems to large regional grids, are typically managed by a central controller that requires complex communication methods and can be unreliable and pose cyber security risks in certain applications, especially when controlling a larger number of nodes. We propose an inherently robust, scalable method of integration using multiple energy storage systems and distributed energy resources, which does not require any means of dedicated communication. This method moves beyond the paradigm of controlling grid frequency at a fixed value (e.g., 60 Hz), instead allowing the frequency to fluctuate within certain limits (e.g., 59.6–60.4 Hz). With a greater operating range, the frequency can carry necessary information from energy storage systems to highly variable distributed energy resources like photovoltaics, wind, hydro, etc.

Table of Contents

List of Figures

List of Tables

1 Introduction

The electric grid is rapidly transitioning from centralized bulk generation to large numbers of highly variable distributed energy resources (DERs) (NERC 2017). Power systems in transition must meet the same reliability and efficiency criteria as conventional centralized power systems. These criteria include:

- Proper balancing between load and generation. This is normally achieved by proper balancing between load and generation within individual balancing areas and by maintaining scheduled tie-line flows between areas.

- Maintaining power flow below the thermal limits of transmission lines and transformers, controlled when necessary using phase-shifting transformers or flexible alternating current (AC) transmission systems.

- Maintaining voltage levels in the system within allowable limits, normally done using voltage regulators, transformer taps, static volt-amps reactive (VAR) compensators, and synchronous condensers.

On traditional interconnected power systems, these criteria are achieved through different operational procedures, at different time scales, using both economic dispatch and allocation of reliability reserves that need to be both centrally controlled and have means of autonomous response based on local plant level controls (such as primary frequency response, voltage control, etc.).

Maintaining the same level of efficiency and reliability under high shares of DERs requires changes in operational practices because of the variable nature of wind and solar photovoltaic (PV) generation, and changes in reliability requirements to ensure that such systems can survive contingency events and quickly restore normal production following such events. The variability and uncertainty of the system with high shares of wind and solar generation dictate the need to add more flexibility to the system by utilizing more flexible conventional generation, responsive loads, and energy storage systems (ESS).

A fundamental limitation of power systems with high shares of DERs that use conventional grid-following converter technologies is their inability to ensure stable grid operation when the voltage source generation capacity diminishes (Lin et al. 2021). This fact is rarely discussed by the greater renewables integration community, but adequate capacity of grid-forming sources has proven more important for stable grid operation than the emulation of large inertia constants by current source converters (Matevosyan et al. 2022). The network cannot stably operate without sufficient voltage sources regardless of how much inertia is present. Alternatively, systems without inertia and high rates of change of frequency (RoCoF), but with enough grid-forming capacity, can still operate in a stable manner if proper controls are implemented (Eto 2018), from which we can conclude that in future scenarios, grid-forming may be more important than inertia.

Grid-forming inverters are also capable of providing all existing and future advanced reliability services similar to or better than any conventional technology, and they help to enhance grid resiliency and security by providing other services, such as islanded operation, black start, etc. In this regard, grid-forming resources, such as grid-forming battery energy storage systems (BESS), can be considered a critical component of power systems of any size that are undergoing transitions to high shares (up to 100%) of inverter-based resources (IBRs). This work is focused on an innovative use of grid-forming IBRs to provide reliable operation of power systems with no conventional (fossil-fueled) generation. We demonstrated our method at the multimegawatt scale using the islanded grid at the Flatirons Campus of the National Renewable Energy Laboratory (NREL), following a real-life contingency event. We then continued the analysis through consecutive, real-time simulations using a real-time model of a larger power system. Detailed descriptions of these activities and results are described throughout this paper.

2 Rationale and Proposed Method

Most existing analyses assume that in the future electric grid, ESS and DER operations will have to be coordinated to assure robust overall system operation, which increases reliance on communications and control systems (Abrahamsen 2021). Power systems of all sizes are traditionally managed centrally (DOE 2015) (Figure 1a), which could be computationally impractical for large numbers of DERs. As the number of grid-edge nodes increases exponentially, these controllers will require increasingly complex communication methods, which could become unfeasible and/or pose cybersecurity risks (Johnson 2020).

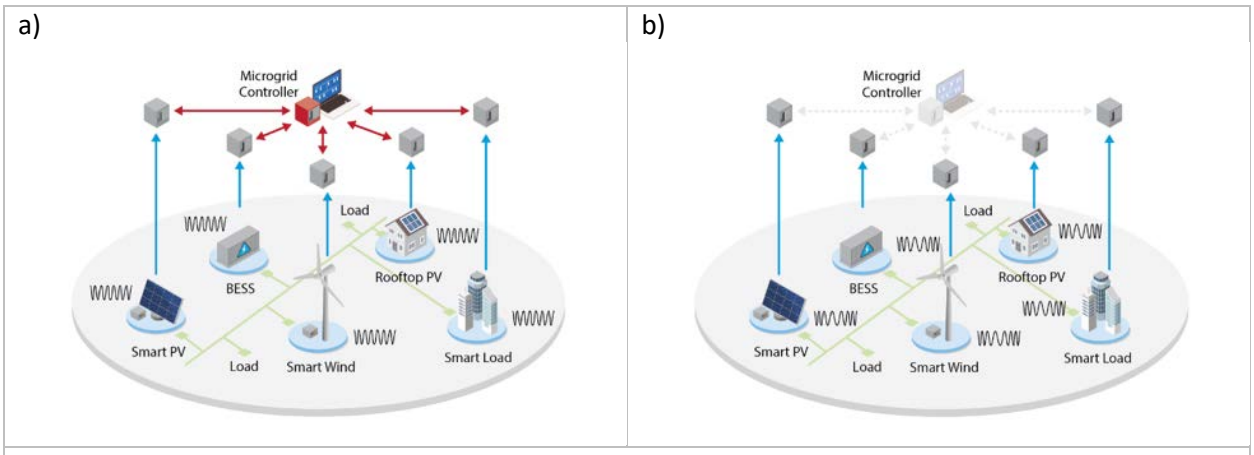

Figure 1. A centrally controlled power system with fixed frequency (a) and (b) a decentralized, communication-less power system.

To overcome these challenges, we propose an inherently robust, scalable method of integrating multiple ESS and DER systems that does not require any dedicated communication means (Figure 1b). Our method breaks from the paradigm of controlling frequency to fixed values (e.g., 60 hertz (Hz)) and assumes frequency can be allowed to fluctuate within certain limits (e.g., 59.5 Hz–60.5 Hz) to carry necessary information about the state of the overall power system between ESS and DERs (Figure 3).

Our method assumes that all devices participating in the scheme are following frequency-power droop. There are multiple definitions of grid-forming inverters depending on the capability being provided (Huque 2021); this paper will assume that grid-forming inverters watch their power consumption and state of charge and adjust the frequency accordingly, as shown in Figure 2a, whereas grid-following devices measure frequency at their terminal—typically using a phase-locked loop (PLL)—and adjust power production accordingly, as shown in Figure 2b.

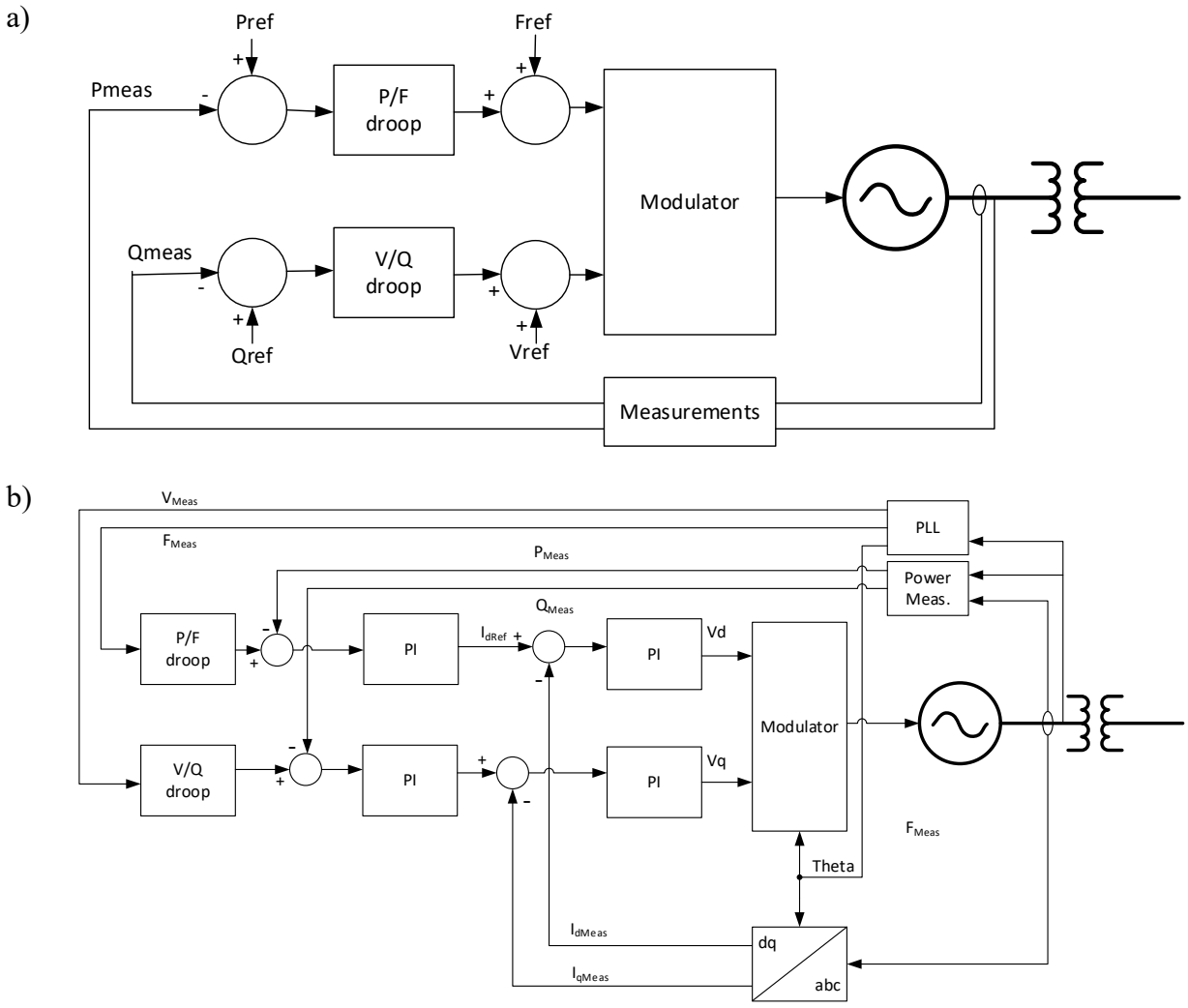

Figure 2. Example implementation of grid-forming (a) and grid-following (b) inverter control.

This power systems control scheme applies to 100% inverter-based generation (IBG) systems in which a great number of highly variable DERs (such as PV, wind, and hydroelectric) are connected to various grid-forming ESS (such as BESS and hydrogen storage solutions), while supplying variable system loads.

Figure 3

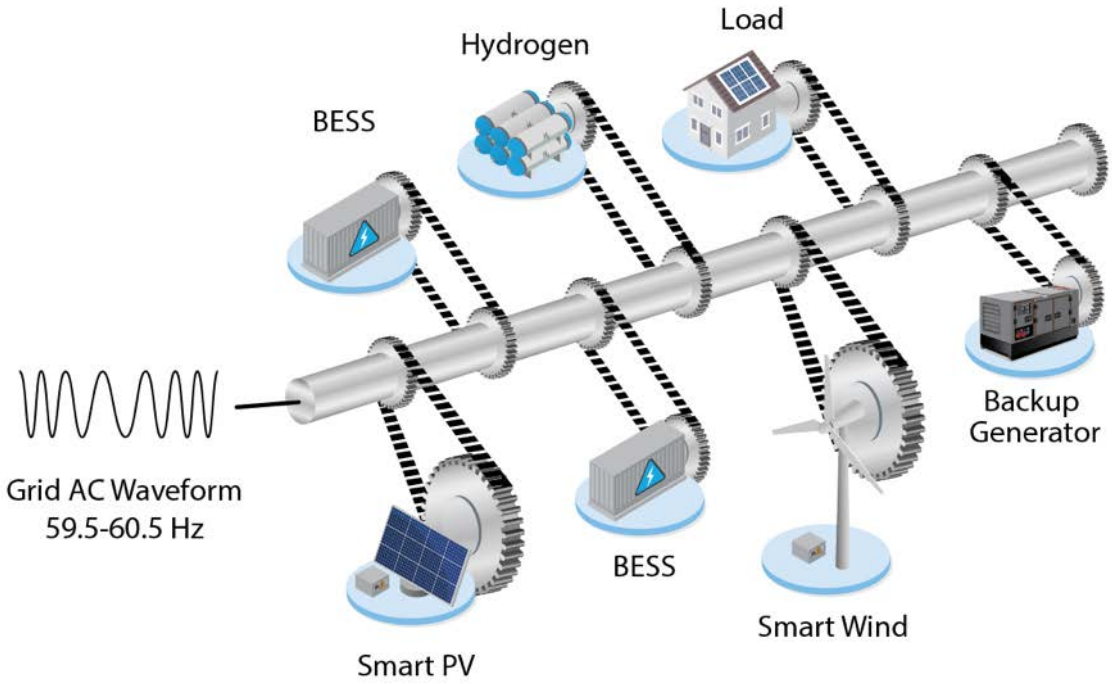

Figure 3. All devices connected to a single power system share the same frequency.

In the short term, the most likely uses for this method are systems that are nearing 100% IBG—such as modular microgrids, plug-and-play systems, black start/failsafe operation (in case of communication loss), and disaster recovery. Multiple aspects of this concept can potentially be adapted by larger island systems and, eventually, regional grids, because it integrates well with conventional generation schemes and can be used as an intermediate step before reaching 100% IBG.

The concept was demonstrated during an unexpected and total loss of grid connection at NREL's Flatirons Campus in September and October 2020 (see Section 3) in which a 1-megawatt (MW) BESS, 430-kilowatt (kW) PV array, and 1.5-MW wind turbine supplied power for an extended time to all loads on the campus microgrid. The energy resources used frequency to ensure that the BESS was not overloaded when excess wind was available and that the Li-ion battery was never overcharged or entirely discharged, as described in Sections 4 and 5. We performed further simulations using a 9-bus model of a 315-MW power system deployed in a real-time digital simulator (RTDS). These simulations showed that our method can scale-up to multiple ESS and that DERs can operate together with conventional generation at various levels of ESS and renewable penetration, as shown in Sections 6 and 7. Our results show that a communication-less scheme, in which the grid frequency becomes the only means of "communication," is a functional design for failsafe grid operation. This method ensures a baseline level of resilience and reliability using only native controls of distributed energy resources, and avoiding requirements for complex and centralized communications.

3 Substation Failure

Figure 4. The 115-kV potential transformer that failed, shown here during substation construction.

In the summer of 2020, NREL had commissioned a new, 115-kilovolt (kV) substation infrastructure to support research on energy systems integration at scale. The infrastructure includes two 25-MW transformers and typical substation-grade protection devices. The substation is grid-tied to utility Xcel Energy's network via a 115-kV transmission line, acquired by NREL for large-scale power grid integration research. Located on the campus, a 7-MW controllable grid interface with an independent research bus allows NREL to perform simulated grid testing using the incoming grid power. The rest of the Flatirons Campus contains more than 10 MW of solar, wind, BESS, and dynamometer resources. An express purpose of the new infrastructure investments was to validate high-renewable systems operating as microgrids, providing black start capabilities, and enabling stability with low system inertia. The substation investment represented a scale-up in U. S. Department of Energy (DOE) power system research capabilities and was deployed as part of the Advanced Research on Integrated Energy Systems (ARIES) research platform.

Figure 5. Security footage at NREL's Flatirons Campus capturing the moment that a 115-kV potential transformer exploded, causing a power outage.

In September 2020, shortly after installing and commissioning the new infrastructure, a 115-kV potential transformer (Figure 4) failed, causing an explosion (Figure 5) that disabled the substation infrastructure and cut power to the Flatirons Campus, which, in addition to the research assets, also includes staff offices and buildings that average about 300-kW in site load with peaks up to 600 kW.

The Flatirons Campus used emergency backup diesel generators to power a limited subset of the campus buildings in the interim. Meanwhile, the substation would remain out of order until a new potential transformer could be acquired and installed. The event halted all high-power systems research at the laboratory, but did not stop researchers from pursuing their ideas about how to restore power to the campus.

4 Microgrid Setup Using Research Assets

The Flatirons Campus contains a suite of grid research assets that are always connected to an isolated "research bus"—none of which were intended to be used for site loads always separated at a "building bus". However, in the wake of the potential transformer failure, the authors of this paper proposed to tie the research and building bus, thereby using the research assets to power the campus in a microgrid. Specifically, we proposed using a 430-kW PV array, a 1-MW/1-megawatt-hour (MWh) Li-Ion BESS, and a 1.5-MW wind turbine to form a renewable microgrid that could power the entire campus independent of Xcel Energy (Figure 6).

This solution was easier proposed than approved, because no prior DOE procedure existed for this type of event. A further challenge to repowering in this way involved contractual agreements between DOE and Xcel Energy, specifying which assets were to be used exclusively for research. Technically, this approach was also challenged by lack of control and monitoring infrastructures that had been disabled as well as outstanding questions, such as whether the system configuration would be stable, whether a possible fault event would endanger staff, and how to manage the BESS for sharing power to loads.

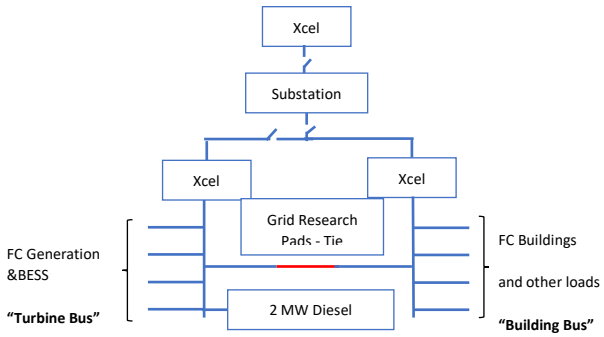

Figure 6. Simplified one-line diagram of the NREL Flatirons Campus microgrid configuration.

The proposed renewable microgrid system was reviewed by a gathering of NREL and DOE staff, including site operations and environmental and health safety teams. A protection scheme was also documented and vetted to ensure safety to staff personnel. Xcel Energy granted permission to tie the building and research busses together while the substation was isolated from Xcel's network, initiating a connection behind the Xcel meters at NREL's grid research pads.

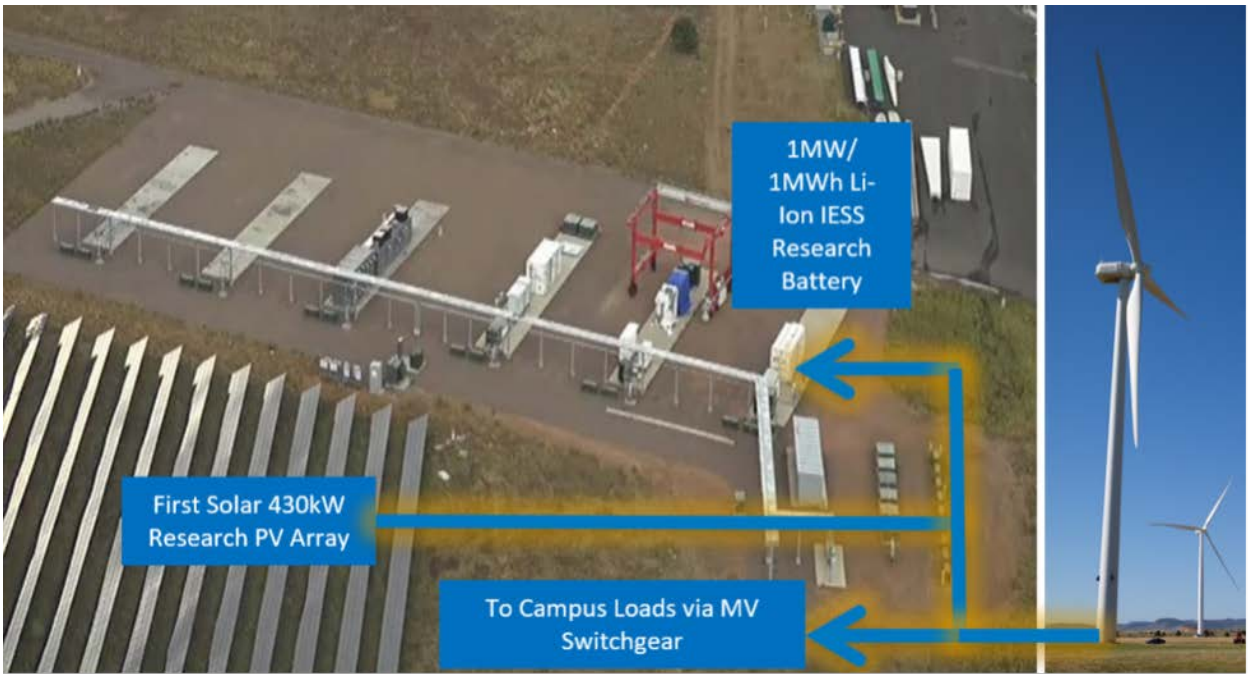

Figure 7. An aerial view of several of the Flatirons Campus microgrid assets that were deployed to power the research campus following a substation failure that cut power from the grid to the campus.

Because available resources and storage were not enough to allow for reliable continuous operation, NREL also rented a 2-MW diesel generator that was integrated into the renewable arrangement, which led to further questions around how to best incorporate the generator. A simplified diagram of the initial microgrid configuration is shown in Figure 7.

With final approval, we proceeded with the attempt to black start the voltage on campus. Even though our main 1-MWh battery was at a good state of charge at 85%, we were not able to execute a black start right away because many subsystems needed to operate the system were not functional:

- The Battery Management System (BMS) was connected to an uninterruptible power supply (UPS) whose battery was discharged
- The Sitewise centralized Real-Time Automation Controller (RTAC) was not able to communicate to the BESS because the communication infrastructure relied on grid power (e.g., network switches)
- The grid integration control center including all of the desktop computers and control screens, were down (i.e., nonfunctioning).

To overcome these issues, we moved multiple UPS systems to buildings with emergency generators to recharge them. Then the UPS were brought back to their original location. Because some of the UPS were only allowing about 45 minutes of operation, we had to coordinate their startup and work quickly to finish power restoration within this time block. Because the RTAC was not operational, we couldn't use our Supervisory Control and Data Acquisition (SCADA) screens to start the battery as we normally would. Instead, we implemented basic scripts on a laptop connected locally to the BESS switch. These scripts would first manually close contactors

of all of the battery strings, then configure the inverter to grid-forming mode and start it. Because most loads on our site had never been connected to inverter-generated voltages, we carefully connected small pieces of the power system at a time. We started by energizing the control center so that we could get visibility into the system's status and proceed with energizing the remaining elements of the system. Voltage generated by inverter voltage has very good quality; therefore, we did not experience issues with powering the system loads. Startup of the large transformers was flawless, despite their total rating of 8 megavolt-ampere (MVA), which exceeded the BESS rating of 1 MVA. There were no in-rush currents due to the voltage ramp-up performed by the inverter (Figure 8). Once the BESS was able to energize the distribution circuits of the Flatirons Campus all the way to the PV inverters, they were allowed to start and inject power to the BESS.

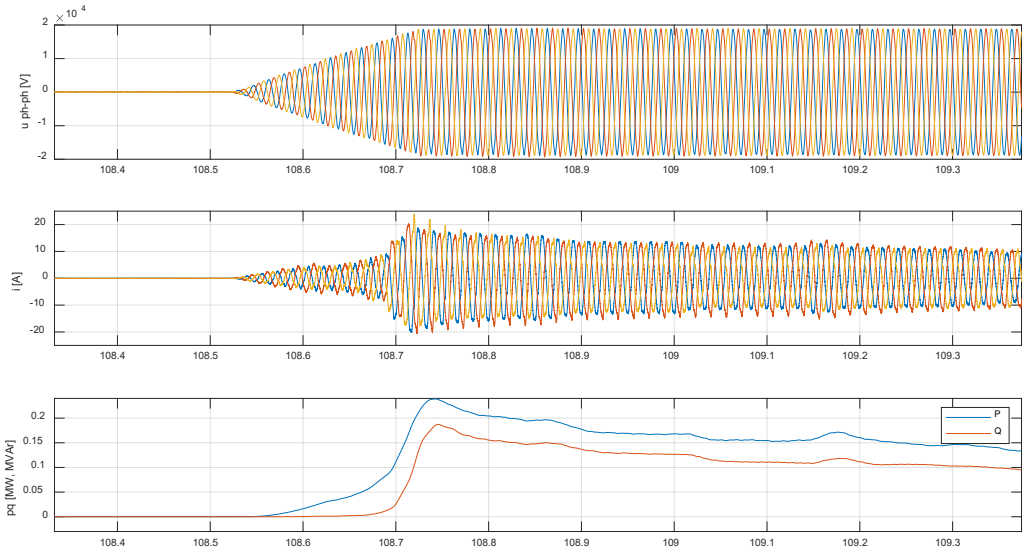

Figure 8. Black start of multiple loads and about 8 MVA transformers using 1-MW BESS.

Remaining sections will explain the communication-less, frequency-based algorithms used for renewable assets management and discuss how our team later validated this approach on a simulated larger-scale system, demonstrating a novel communication-less approach to managing high or fully renewable power systems.

5 Frequency-Based Algorithm for Communication-Less Microgrid Operation

After we verified that the battery could form the grid and the PV could inject power to the battery, we encountered the following challenges:

1. How do we ensure the PV doesn't overcharge the battery?
2. How do we ensure that if PV and wind work together (combined average power of 2 MW), we don't exceed maximum battery-charging power?

These functionalities would typically be managed by microgrid controllers, but we did not have a microgrid controller available; developing a controller on such short notice was not a viable option. Instead, we developed a communication-less scheme that took advantage of generic and distributed frequency controls on the renewable assets that were already available as standard functionality of these inverters.

5.1 Operation with BESS and PV

Because the PV system rating of 430 kW is nearly twice the typical load, it only took a few hours to fill the battery. At this point, we needed to develop a way to inform the PV inverters to curtail power production without using communications or a central controller. To explain our method, we will first summarize the BESS and its controls. NREL's BESS control system consists of three independent controllers (Figure 9):

- Inverter controls: These are provided by the inverter manufacturer and allow for grid-forming operation in either grid-connected or islanded condition, using droop approaches as employed in our recovery. Figure 9 shows how active power P_{meas} measured at inverter terminals is multiplied by the droop coefficient K_{FP} to calculate a frequency reference setpoint F_{ref} for an internal oscillator. The oscillator then generates an instantaneous voltage setpoint for the inverter's phase width modulation (PWM) circuit.

- Battery Management System: The BMS is provided by the battery manufacturer to monitor the status of batteries. Based on measurements of cell voltages and currents, the BMS estimates actual state of charge (SOC).

- BESS controller: This was implemented by NREL using an RTAC controller, which integrates inverter control and the BMS. One of the functions of our BESS controller is to ensure the battery is not over- or under-charged. This is achieved by a limiter that increases P_{set} gradually when SOC increases above a certain threshold, causing the inverter to limit its charging power (or increase frequency setpoint in grid-forming mode). On the other hand, when SOC falls below a set threshold, a P_{set} adder gradually decreases, causing the inverter to limit its discharging power (or decrease the frequency setpoint in grid-forming mode).

In practice, a commercial battery will likely consist of the same components and should allow the same functionality that was used in our recovery. This is discussed further in Section 8.

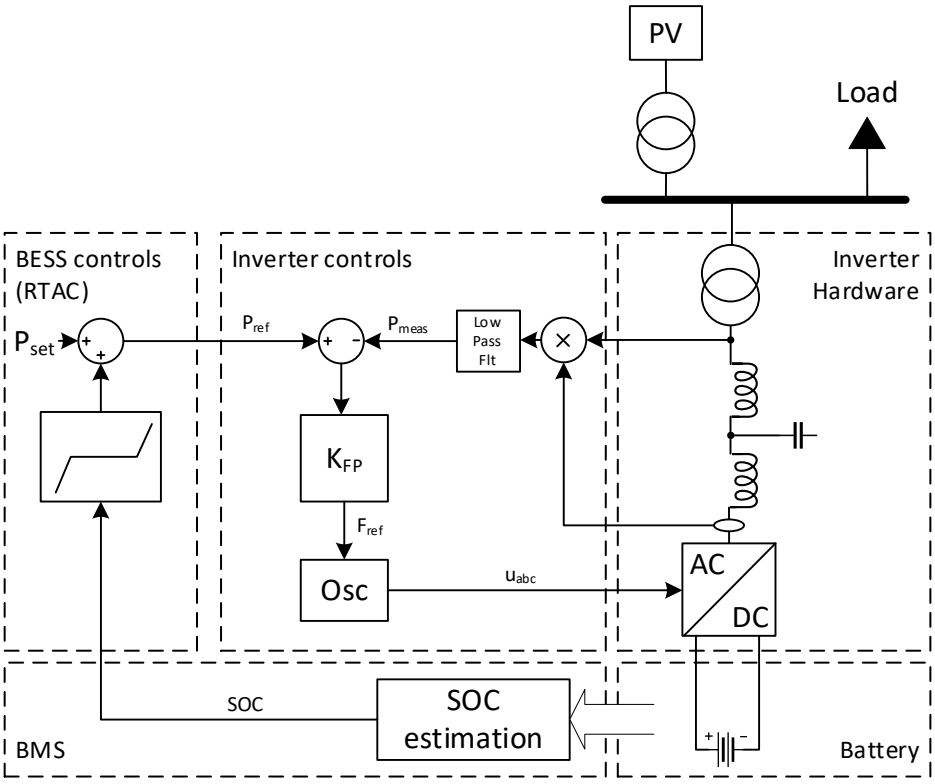

Figure 9. Overview of active power and frequency controls of NREL's BESS system

Figure 10 shows the dependency of active power on frequency for PV and BESS, the only assets connected at this stage. The BESS inverter droop K_{FP} was configured at 0.43 Hz/MW, shown as a relatively steep slope of green lines. Multiple BESS lines correspond to the mechanism of droop curve shifting caused by high or low battery SOC. For a wide range of SOC, between 10% and 85%, we used a middle droop curve. Above the threshold of 85%, we shifted the droop curve to produce higher frequencies, thus pushing system frequency toward the PV curtailment zone.

Blue lines show curtailment characteristics of the PV system, which are implemented in the PV inverters as a standard grid support function. Multiple lines correspond to the fact that full power is not always available; depending on available solar resource, the appropriate curve has to be selected. All curves merge however in the PV curtailment zone above 60.13 Hz. If frequency were to rise above 60.6 Hz, PV would cease generating and there would be no remaining generation, thus no risk of BESS overcharging. Load lines are flat because loads were not capable of supporting the frequency-active power scheme at this point, such as under-frequency load shedding and smart loads, as described in Section 6.

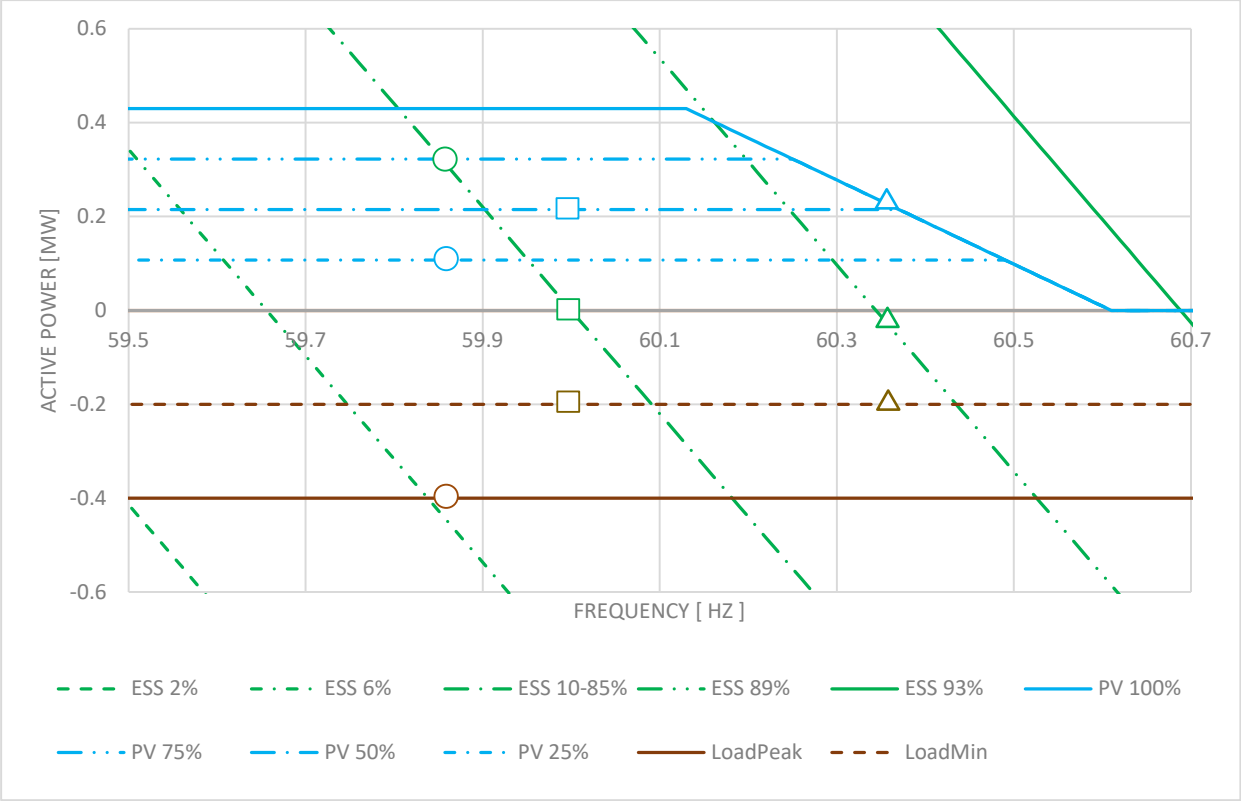

Figure 10. Droop control scheme for PV and BESS during initial system setup. The vertical axis is active power of a given asset and the horizontal axis is frequency at the devices' terminals. Multiple lines for ESS show droop curve shifting for various SOC levels. Multiple lines of PV show characteristics depending on available solar power (25–100%). Expected minimum and peak loads are also plotted.

As long as the sum of all curves used is monotonically decreasing with increasing frequency, Figure 10 can be used to determine frequency and active power given the battery SOC, available PV, and load. The principle is that for a given SOC and available PV power, the sum of all powers injected into system must equal zero, as in (1).

$$P_{ESS}(F, SOC) + P_{PV}(F, P_{Avail}) + P_{Load} = 0 \qquad (1)$$

Three examples for determining the power state are shown in Figure 10.

- In the first case (marked with circles), PV is at 25% available power (107.5 kW), SOC is 10–85%, and load is at its peak (-400 kW). The system will stabilize at around 59.85 Hz with the battery beginning to discharge at 292.5 kW.

- In the second case (marked with squares), the loads reduce to -200 kW and available PV increases to 50% (215 kW), while SOC stays in the same range. The system will stabilize around 60.01 Hz with the battery beginning to charge at 15 kW.

- In the last case (marked with triangles), the loads stay at 200 kW and available PV increases to 100%. SOC is now high at 89%, so the green line second from right should

be used for the battery droop curve. We can determine that frequency will increase to around 60.35 Hz, the battery begins charging at around 30 kW, and PV is curtailed down to around 230 kW.

Using these exact setups and droop settings, we observed successful, automatic and communication-free restriction of PV generation such that BESS SOC never exceeded 93% (Figure 11). The figure shows actual measurements of one sunny day during this early stage of our microgrid operation. At the beginning of the day, when loads were connected, there was not enough PV, so the battery discharged from 85% down to 50% at 9 a.m. At this point, PV production exceeded load and the battery started charging. Around noon, it is visible that upon reaching 85% battery SOC, the frequency increased as expected and PV production was curtailed down to ca 250 kW, thus matching load. Since generation nearly equaled load, the battery stopped charging at this point and stabilized the SOC at ca 89%. The measured frequency and power distribution is in line with droop scheme presented in Figure 10. All of this being achieved with just frequency as the "communication" method.

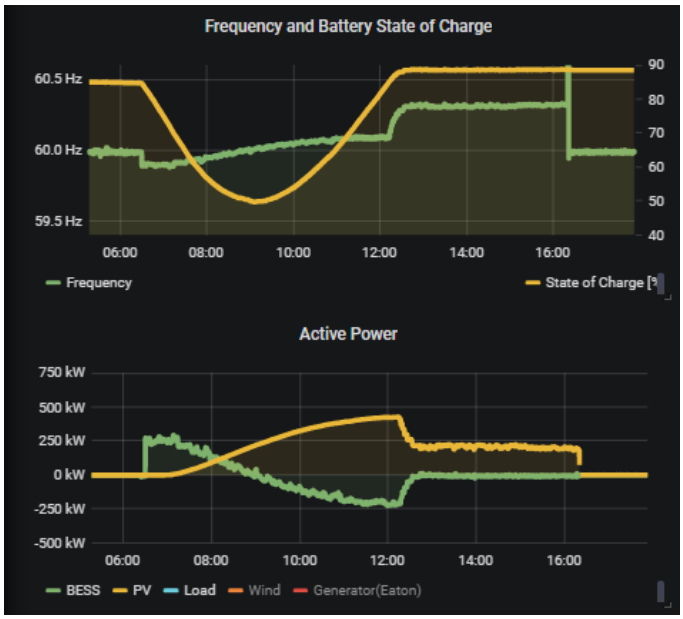

Figure 11. Frequency and power of PV and BESS during a 12-hour cycle using a frequency-based, communication-less control scheme.

5.2 Adding 1.5 MW of Wind Power to the Mix

Having established a functional PV-BESS operation scheme, we then proceeded with interconnection of a 1.5-MW wind turbine—to provide power overnight when wind is available. Because the configuration had never been tried before, a step-by-step energization procedure was developed taking into account a possible unstable operation and additional precautions. Once again, the addition of wind raised the challenge that would typically be handled by a central microgrid controller: On top of a need to prevent battery overcharging, we had to take special care not to exceed the BESS maximum rated power of 1 MW, which could easily be exceeded with total generation of 2 MW and load as low as 250 kW at times. The battery inverter is oversized compared with the battery's continuous power by a factor of 220%; it also allows for

150% short-term overcurrent, thus allowing our team to supply 330% overcurrent in case of short power spikes or in-rush currents. That capability allowed a bit of flexibility in designing a communication-less control scheme because short power spikes on a battery were acceptable. Oversizing the inverter is a recommended, if not required, feature for implementing this scheme.

Prior to deploying the new configuration, we developed a model that allowed simulation of frequency and power flows in the system (Figure 12). It is applicable to systems with a single BESS and multiple generation resources, and with simulated loads to evaluate the performance of our frequency droop scheme. We then ran the model on an example scenario with variable wind and PV and with loads changing in steps (Figure 13).

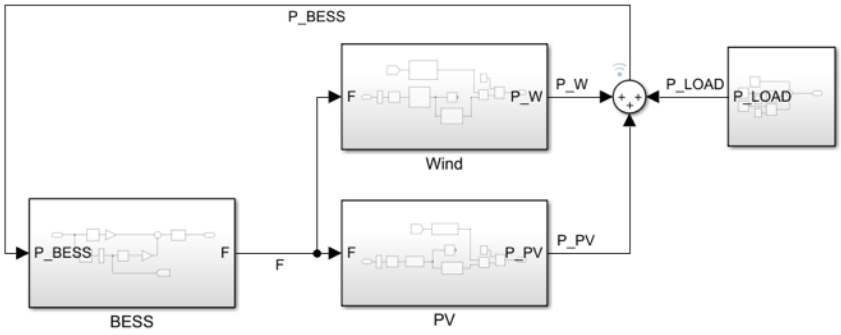

Figure 12. Simple model for evaluating the performance of our frequency droop scheme using a BESS, multiple generation resources, and simulated loads.

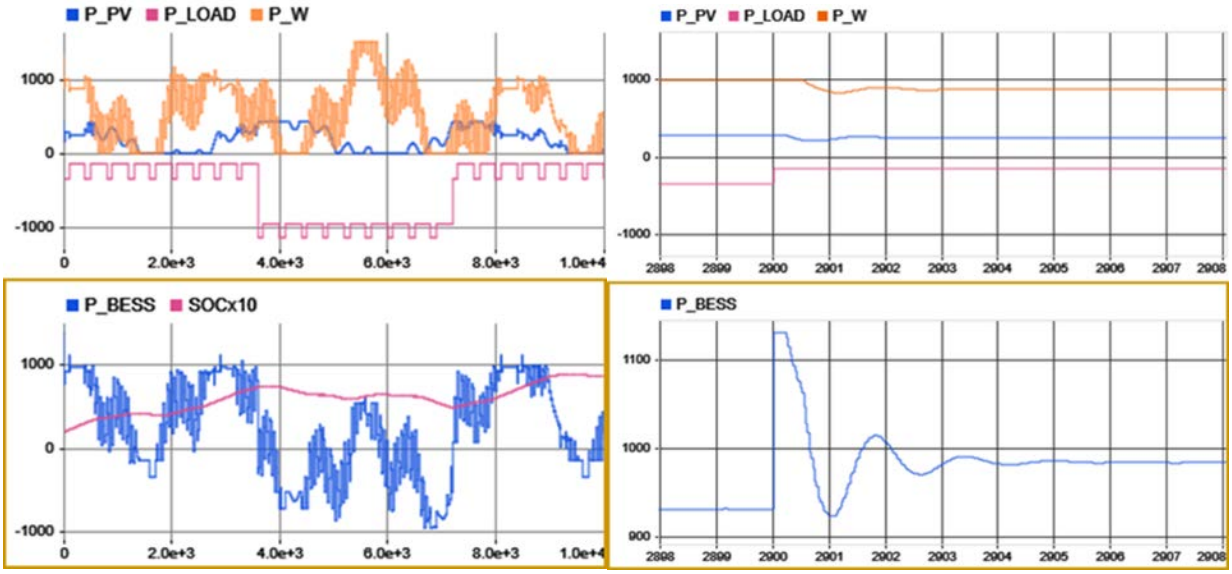

Figure 13. A scenario of our model using variable wind, solar, and load conditions. The vertical axis is power, the horizontal axis is time.

A PV and wind profile was implemented as a combination of sinewave profiles with random magnitudes and frequencies, so that it was more variable than the power profile based on historic data at the site. Also, the frequencies were selected so that, at times, all combinations of PV and wind conditions were existent, ranging from no renewable production to full power conditions

from both assets. At the same time, load was programmed with 200 kW of load steps performing periodically—as can be expected at our site due to certain electrical heating processes. Load was also simulated at higher-than-expected levels in preparation to operate with additional load bank to demonstrate operation of renewables at full power.

The simulation demonstrated that our communication-less scheme was robust and could provide 100% renewable operation in all conditions expected, while at the same time making sure battery SOC was not exceeded and the BESS active power rating of 1 MW was not exceeded. Short spikes corresponding to large load steps are visible, which exceed the 1-MW BESS rating for a very short time; this behavior was expected and handled by the BESS overcurrent capabilities.

The above simulation also allowed us to fine tune parameters of BESS, PV, and wind droop curves as shown in Figure 14. Here, BESS droop has been configured more aggressively at 0.28 Hz/MW and both PV and wind are set with more aggressive droops of 0.2 Hz/pu (per unit). Since both PV and wind were sharing the exact same droop characteristics, these are shown combined in the below figure with rated power of 1.93 MW.

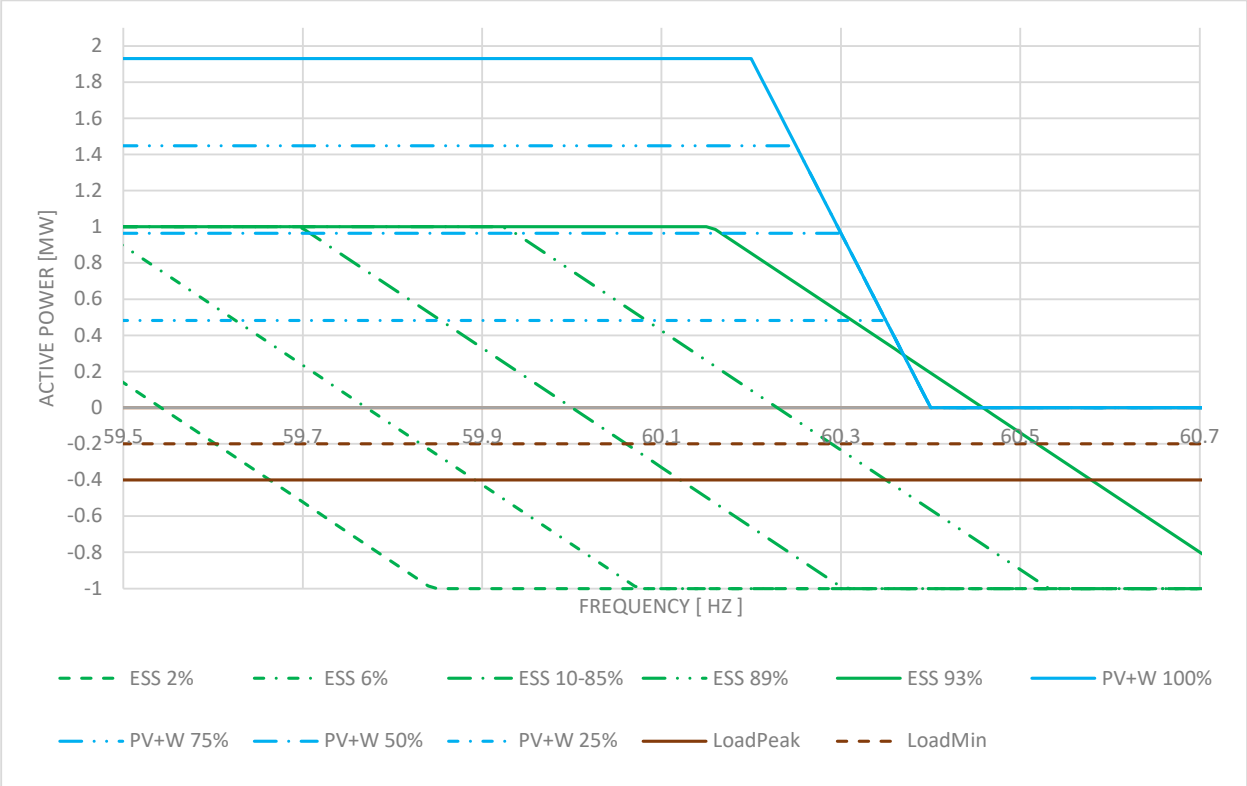

Figure 14. Our droop control scheme for the BESS, PV, and wind system setup.

The above chart can be confusing, thus a different set of plots can be derived by solving equation (2) for frequency, assuming certain parameters for P_{Load} (in our case 0.3 MW) and for SOC and P_{Avail}.

$$P_{ESS}(F, SOC) + P_{PV+W}(F, P_{Avail}) + P_{Load} = 0 \qquad (2)$$

After solving for frequency, the active powers of the battery, PV, and wind can be easily calculated and plotted as shown in Figure 15. The top left subplot shows that estimated frequency in this system should never exceed 60.5 Hz when the battery is in SOC-limiting mode, and should not exceed 60.3 Hz while the battery is charging. The top right plot is important because it confirms that even with nearly 2 MW of available wind and PV power, battery power shall never exceed its rating of 1 MW. The plot also shows a white horizontal area where battery is at zero power near 92% SOC, indicating that with high available PV and wind power, SOC should stabilize at this level and not cause battery overcharge. The bottom left subplot shows combined wind and PV power production. It shows that maximum production is properly curtailed to around 1.2 MW. It also shows power curtailment all the way to 0 MW when SOC of battery is high.

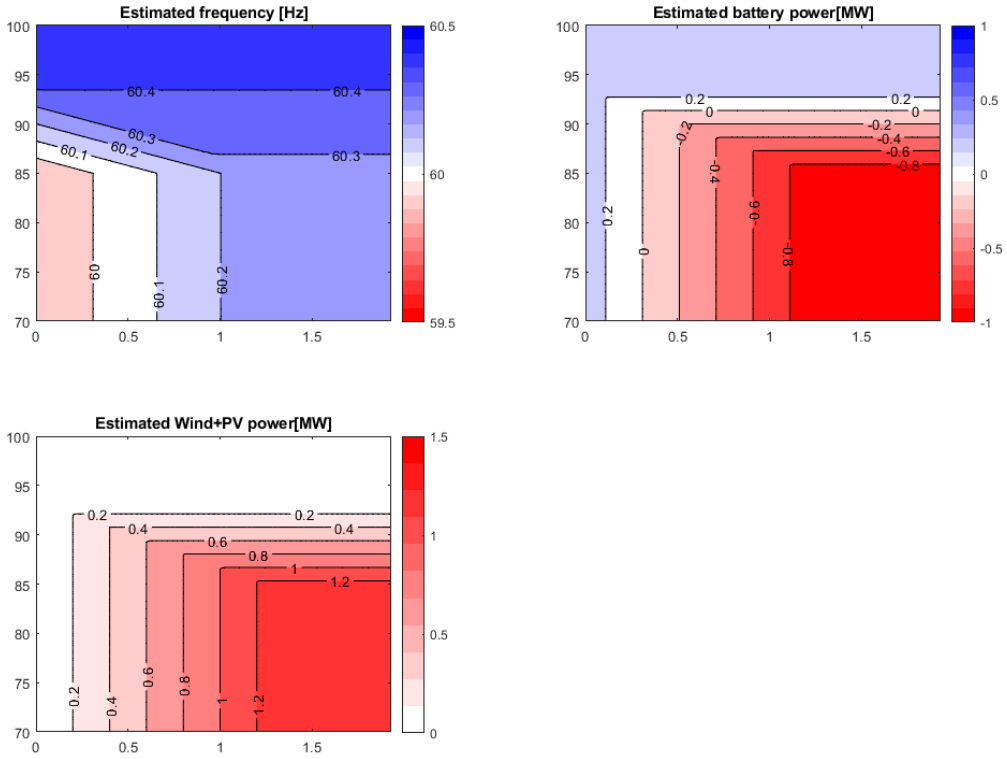

Figure 15. Estimated frequency and power flows to BESS, PW and wind, calculated based on droop settings of devices. The x-axis on all drawings represents available PV and wind power in MW, while the y-axis represents battery SOC in percent. Positive power means discharging (generation) while negative is charging (load).

Following the successful simulation results, we proceeded with connecting a wind turbine to the system. Figure 16 shows a 24-hour period of operation at the Flatirons Campus using only a 100% inverter-based—a 1.5-MW wind turbine and a 430-kW PV system. At 8 a.m., the system started with 50% SOC and the battery kept discharging until 10 a.m. when PV production started exceeding site loads and the battery started charging again. We started the wind turbine at 4:45 p.m., when the wind was very strong, and we were able to charge the battery quickly to 93%. It is visible that as time frequency also increased, curtailment of wind production started. The wind

conditions overnight were variable, with extended periods of no wind at all, where the battery was discharging relatively quickly and random variable wind gusts were captured by the battery and allowed the system to operate through the night. Voltage quality was very good throughout that entire period while frequency stayed between 59.9 Hz and 60.35 Hz. No device on the network experienced an issue with operation at this range of frequency. The system matched our expectations on model predictions very well.

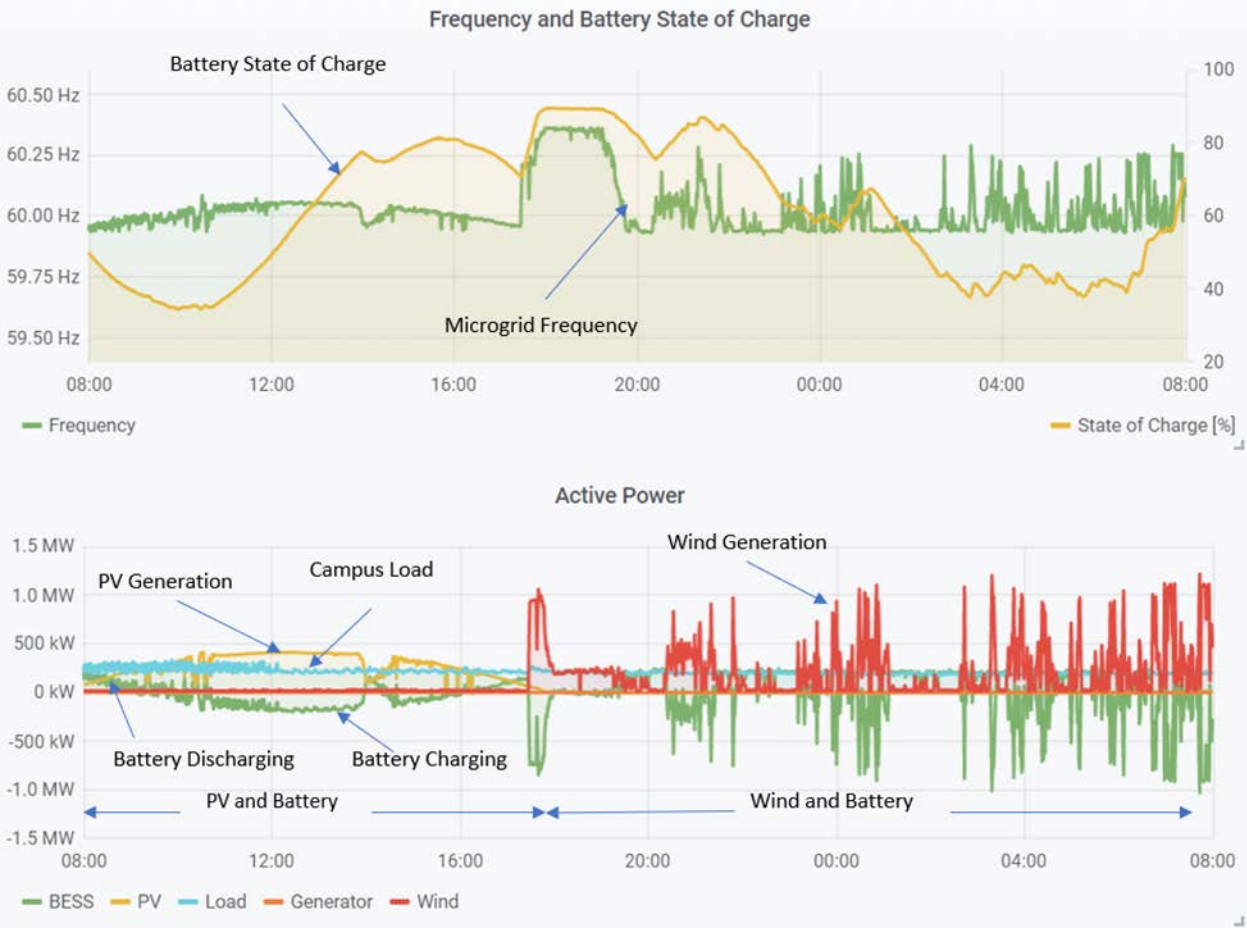

Figure 16. 24 hours of 100% renewable operation at the Flatirons Campus using PV, wind, BESS, and loads in a communication-less control scheme.

5.3 Adding a 2-MW Generator to the Mix

Sometime after the initial microgrid was powered on, NREL rented a 2-MW diesel generator to supply interim power when renewable resources were not available. However, the 2-MW generator operated on a fixed-frequency setpoint and did not have frequency droop capability readily available; therefore, this generator could not participate in the frequency-based control scheme.

Initially, the generator was manually started each time we shut down the battery to take over all loads, then stopped in the mornings when we restarted the BESS setup. Each transition caused a

short, few-seconds-long, blackout to the site that was inconvenient for many devices that lacked UPS.

Following the substation failure, we configured the generator to provide coordinated power with the BESS and successfully configured the system to transition seamlessly between BESS-only mode, BESS-plus-generator mode, and generator-only mode, as shown in Figure 17. Later, an automatic system was developed that started the generator when the battery SOC fell below 20%, allowing quick-charging of the battery at 1 MW up to 90% during a 40-minute period, followed by automatic disconnection of the generator. Because of this arrangement, the diesel generator was operating closer to its nominal power rather than operating near idle while supplying an average 250 kW of loads, which is only 12% of its nominal power.

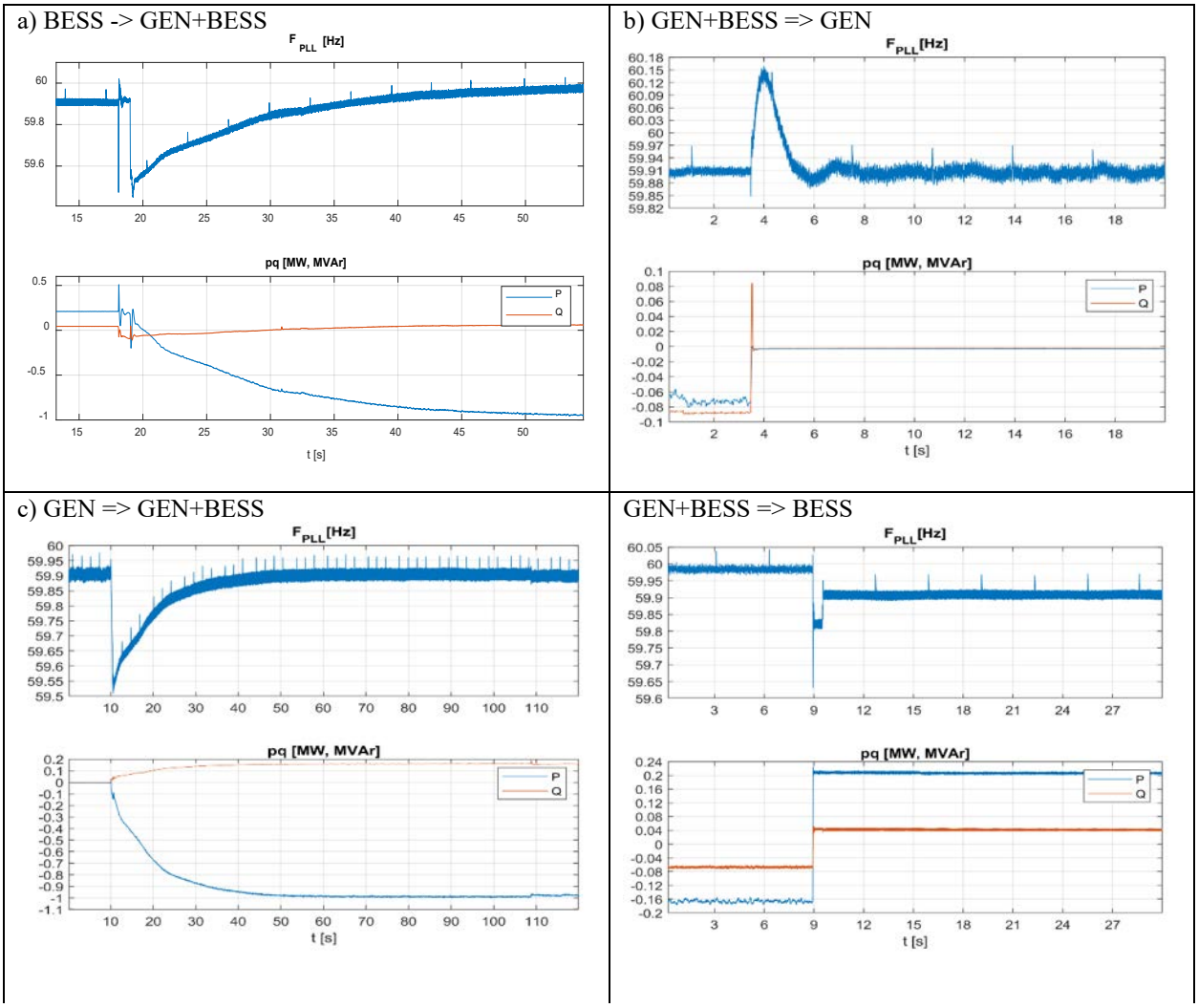

Figure 17. Frequency and power measurements of the BESS during seamless transitions between various operating modes: a) BESS to BESS + GEN, b) BESS + GEN to GEN, c) GEN to GEN + BESS, and d) GEN + BESS to BESS.

For the generator-integrated system, the droop-based controls that were programmed on the BESS and other resources provided resilient backup to the configuration. We encountered a few

issues related to the rental diesel generator tripping-out because of an internal fault. This also happened during the BESS charging period, one of which was captured when the BESS was charging at 1 MW (Figure 18). The figure shows how the BESS instantly can take over 1.1 MW of active power step without causing any noticeable disturbance to the system voltage. The takeover is achieved naturally through a droop-based power-sharing approach and doesn't require any central controller intervention; thus, it adds a level of redundancy to the system where two different technologies, the BESS and diesel generator, work together to assure safe power delivery.

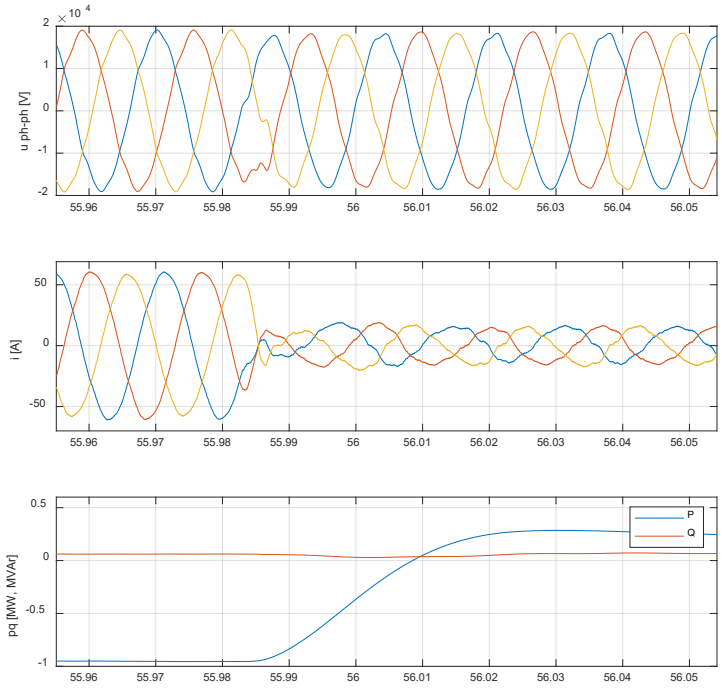

Figure 18. Measurements at the BESS during a drop in generator power because of an internal issue, and the BESS instant takeover of 1.1 MW of active power.

5.4 Summary of Microgrid Operation

The substation outage began on September 8, 2020, and lasted until October 15, 2020. Figure 19 shows the energy generation split by resource, and estimated fuel consumption by diesel generators, as well as estimated savings resulting from renewable microgrid operation. As shown, at the beginning, multiple emergency diesel generators distributed onsite allowed us to power-on a limited set of loads. We then reduced this generator's output once we integrated the PV-BESS system, which provided instantaneous savings in place of using diesel fuel. Shortly after, we rented a 2-MW diesel generator and re-energized the entire site. After we validated the wind-PV-BESS configuration, we initiated full renewable microgrid operation, which operated continuously for around 72 hours near the end of the substation outage. The substation was repaired soon after, and the campus was once again tied to the grid.

Figure 19. Operation of the NREL Flatirons Campus microgrid throughout its more than month-long outage period, showing daily energy production from each generator as well as diesel generator fuel consumption and fuel savings due to renewables and BESS operation.

6 Scaling-Up Communication-Less Controls for Larger Power Systems

Following the success of our communication-less microgrid scheme for restoring power at the Flatirons Campus, we asked whether the same configuration could operate on a larger power system. Instead of only one BESS and multiple DERs, could this scheme work for multiple ESS, DERs, and conventional generation resources? Further, we were interested in whether this approach was feasible at various combinations of renewable penetration levels, ESS penetration levels, and ESS duration defined as:

$$Renewable\ Penetration\ [\%] = \frac{Total\ Renewable\ Capacity\ [MW]}{System\ Peak\ Load[MW]}$$

$$ESS\ Penetration\ [\%] = \frac{Total\ ESS\ Power\ Capacity\ [MW]}{System\ Peak\ Load[MW]}$$

$$ESS\ Duration\ [h] = \frac{Total\ ESS\ Energy\ Capacity\ [MWh]}{System\ Peak\ Load[MW]}$$

To show the method can be used in a wide variety of system configurations, we validated the system in multiple combinations of renewable penetrations, ranging from 20% to 300%, including ESS penetration ranging from 12% to 150% as well as ESS duration ranging from 0.4 hour to 15 hours (Figure 20). The NREL Flatirons Campus case is marked on the figure as a dot in the top-right corner.

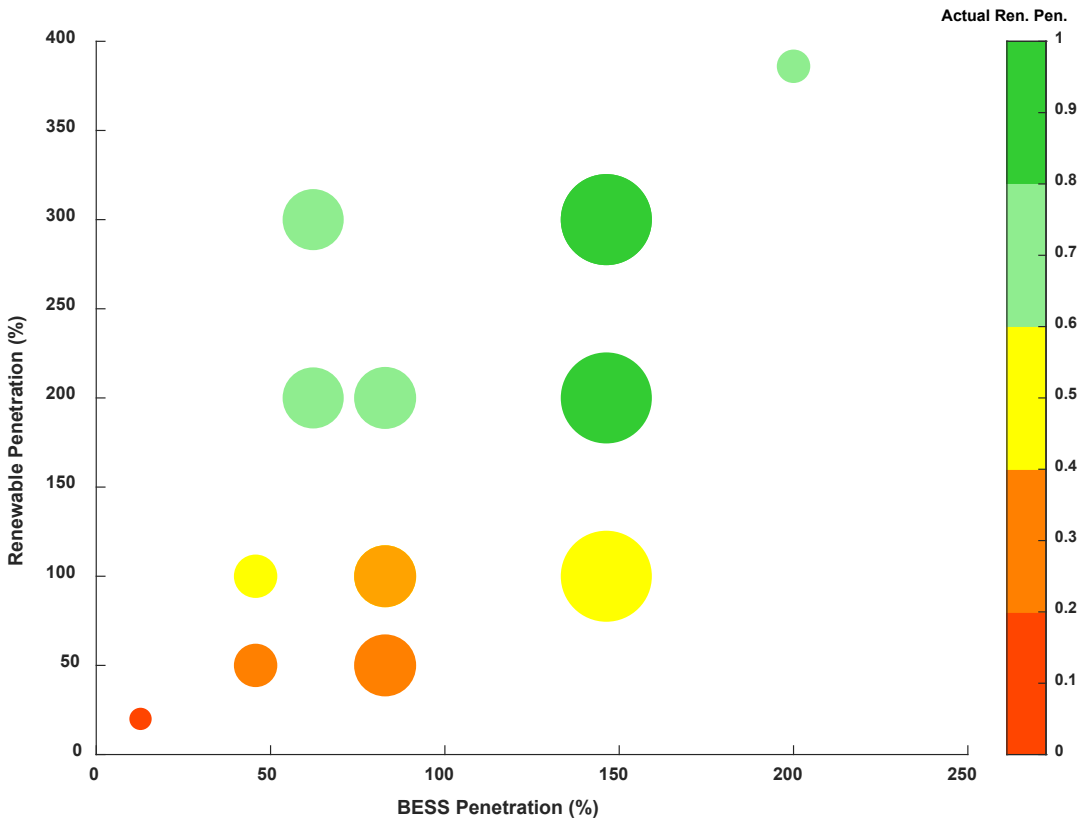

Figure 20. Summary of cases run using RTDS 9-bus simulation model with various levels of renewable penetration (Y axis), BESS penetration (Y-axis), BESS capacity (circle diameter), and resulting renewable penetration (circle color).

A communication-less approach would be important for larger-scale systems because it could overcome the complexity and vulnerability of using a central controller to coordinate the operation of so many DERs. For example, a conventional system configuration would use a central controller to forecast and schedule setpoints to devices, naturally introducing some delay in system response, and reducing the capability to seamlessly integrate other DERs without reconfiguring the system controller. As we experienced with the Flatirons Campus microgrid, a communication-less approach bypasses the need for a central controller, and introduces new benefits related to plug-and-play compatibility and system reliability. In addition, the ESS would inherently be protected against overcharging and completely depleting storage without the need for a central controller to regulate the SOC.

To determine whether this approach is feasible on a larger system, we developed a model with a larger number of resources, including a mix of renewable and conventional generators. Our experiment used the IEEE 9-bus system model in an RTDS with the following assets:

- Three conventional generators with varying dynamic capabilities: 124 MVA (slow), 96 MVA (medium), 64 MVA (fast). To achieve communication-less operation, these were configured as stand-alone generators with frequency and voltage droop, and with automatic start-and-stop logic implemented based on system frequency measured at their terminals.

- Three varying loads with smart capabilities (100 MW/35 Mvar, 90 MW/30 Mvar, 125 MW/50 Mvar nominal)—system peak load of 315 MW
- Nine grid-forming ESS varying in size and storage duration
- Two PV power plants (118 MVA and 16 MVA nominal)
- Three wind power plants (83 MVA, 83 MVA, 16 MVA nominal)

A single-line diagram of the system configuration is shown in Figure 21.

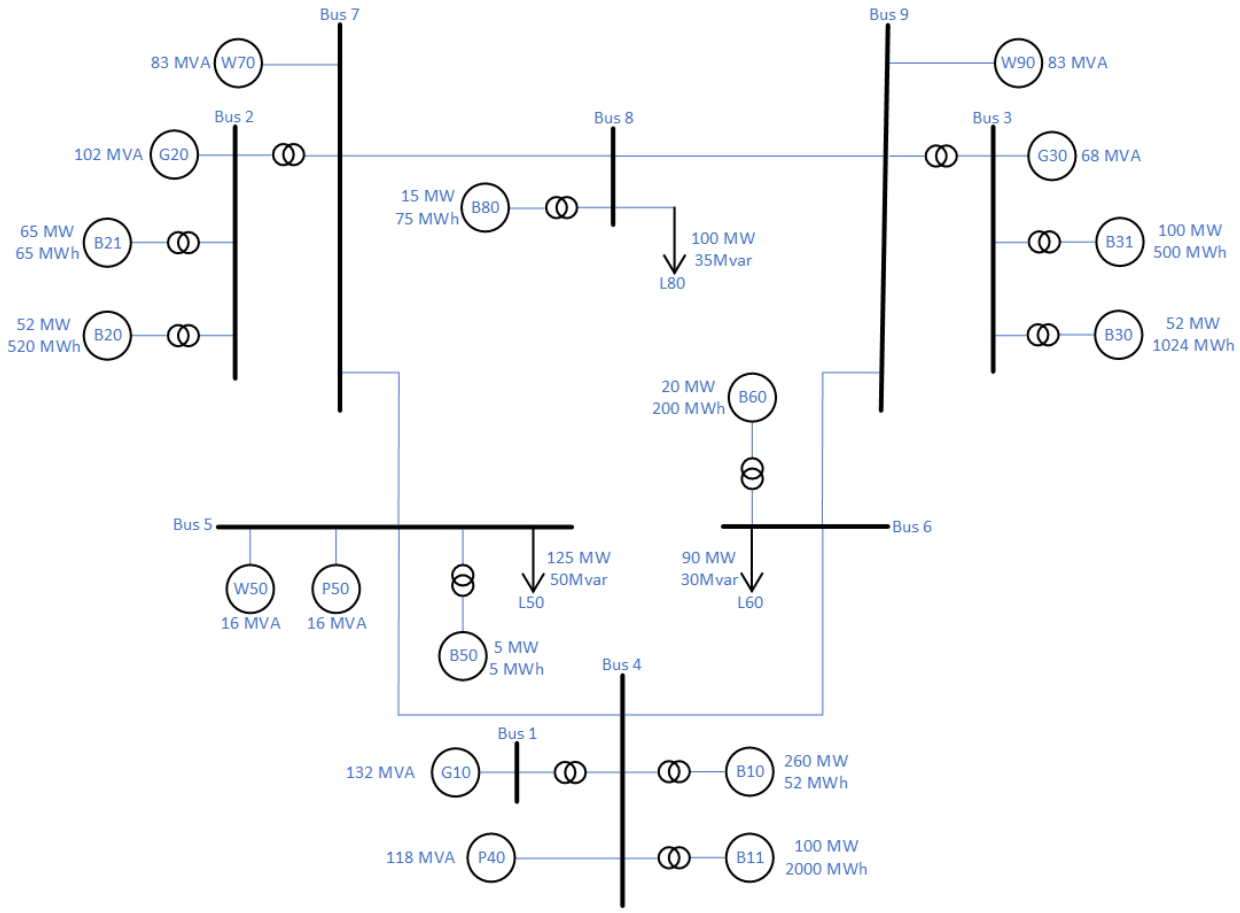

Figure 21. Single-line diagram of simulated large-system communication-less control scheme.

The wind and PV profiles for the simulated assets were derived from actual data measured at the Flatirons Campus. The wind profiles are based on wind speed measurements taken from sensors on a GE 1.5-MW wind turbine with an 80-meter hub height. Available wind power generation was calculated using the measured wind speed and power curve of the wind turbine. Similarly, using irradiance measurements, we calculated available solar power generation. We compiled two profiles: a one-day profile and a one-week profile. Figure 22 shows the one-day generation profile, and Figure 23 shows the one-week generation profile. For the one-day profile, the irradiance measurements were selected from a day with intermittent clouds, and the wind speed measurements were selected during a day with high wind variability. Similarly, the one-week profile contains measurements with high variability. There are also moments within these profiles where there is neither PV nor wind generation available. These conditions were selected as a worst-case scenario for our simulations to validate the robustness of our proposed

communication-less control algorithm. We applied time delays and various low pass filters to reduce overall variability of the resources, which is to be expected with larger plants compared with the single-location capacity at NREL's Flatirons Campus.

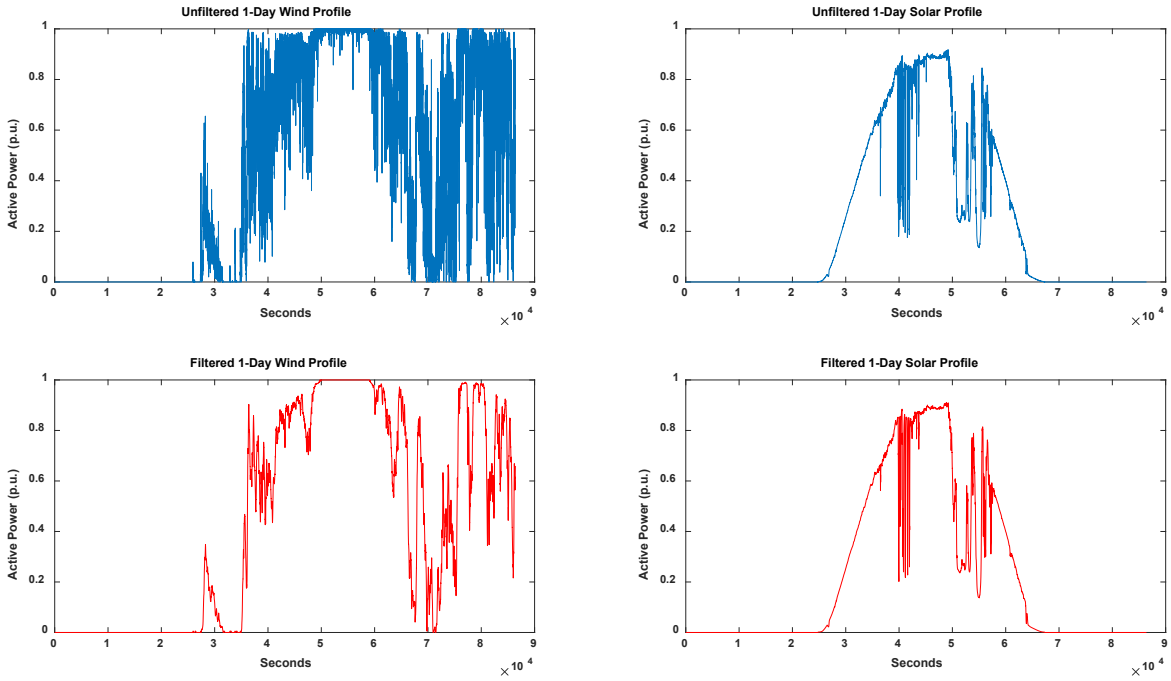

Figure 22. One-day wind and solar generation profiles from real operation at NREL's Flatirons Campus.

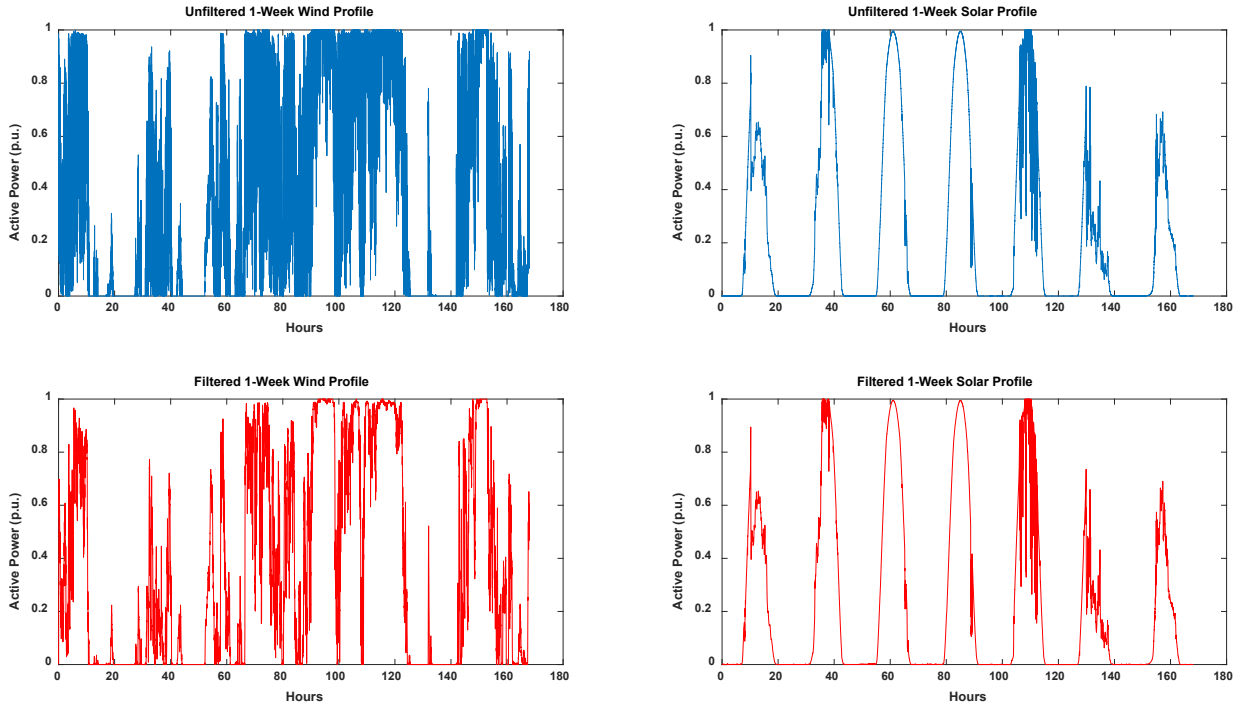

Figure 23. One-week wind and solar generation profiles from real operation at NREL's Flatirons Campus.

We developed three load profiles for the three loads in the RTDS model based on actual load data selected from the New York Independent System Operator (NYISO), shown in Figure 24. The loads were scaled such that peak load corresponds to system peak load of 315 MW. The loads also consisted of 20% "smart" loads—but still communication-less. We envision that certain types of loads (e.g., HVAC appliances) could be required by standards to reduce their consumption in case the frequency drops below a certain level to support the grid without the need for communication to each of these. Already, utilities are incentivizing commercial- and individual-class customers that provide on-call or communication-based voluntary reduction of load demand during peak load times. Additionally, all three loads implemented an under-frequency load shedding (UFLS) scheme where loads decreased in 5% increments as the frequency dropped below certain thresholds as visible in Figure 25. This scheme is well-known in current grids as a way to prevent the entire system from blacking out by disconnecting certain lower-priority parts of the grid.

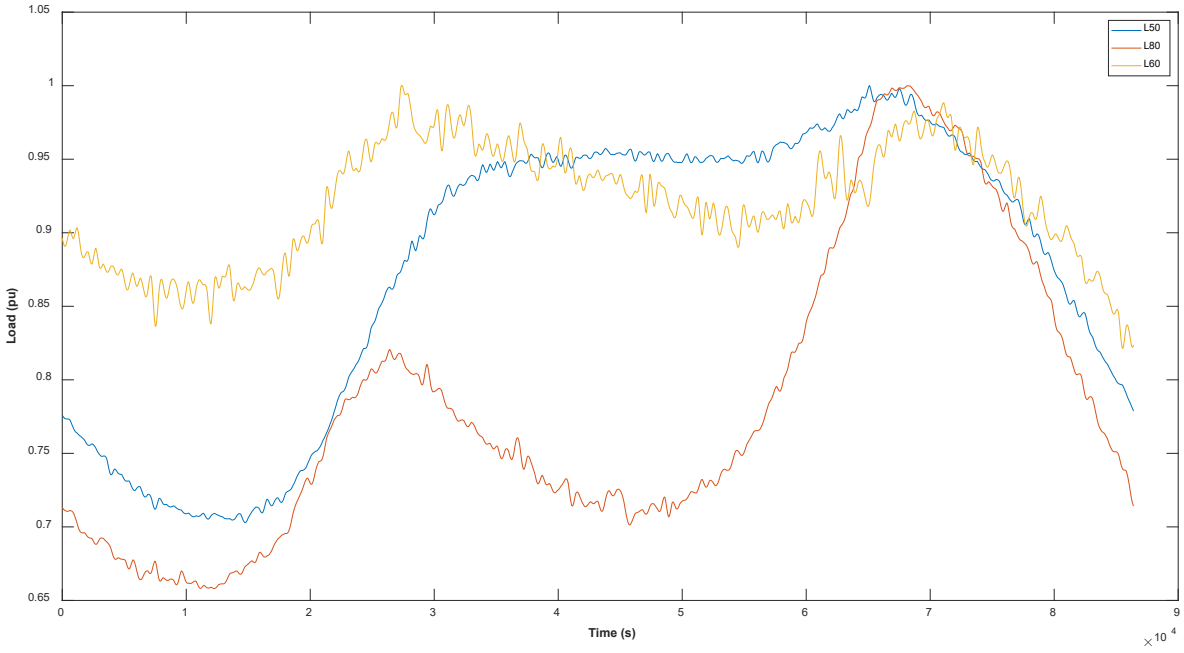

Figure 24. Load profiles based on NYISO example data.

The nine grid-forming ESS inverter models included throughout the 9-bus system are scaled-up and validated models of a commercial SMA inverter that is used with the BESS at the NREL Flatirons Campus. It operates with frequency-power droop of 1.66% and SOC-frequency droop, as described in the previous section. The PV and wind inverters are typical grid-following inverters with a phase-locked loop and frequency-power droops configured accordingly to achieve curtailment. Each of the simulated conventional generators used a different model with different dynamics. These models were enhanced with automatic start/stop functionality based on frequency measurements. Each generator stopped when frequency exceeded the threshold of 60.75 Hz so that they would not operate when renewables are curtailing their production. The stopping delays on these generators were varied to prevent all of the generators from stopping at the same time. Similarly, each generator started when the frequency fell below certain thresholds. The communication-less frequency droop scheme that we employed in this simulation is shown in Figure 25.

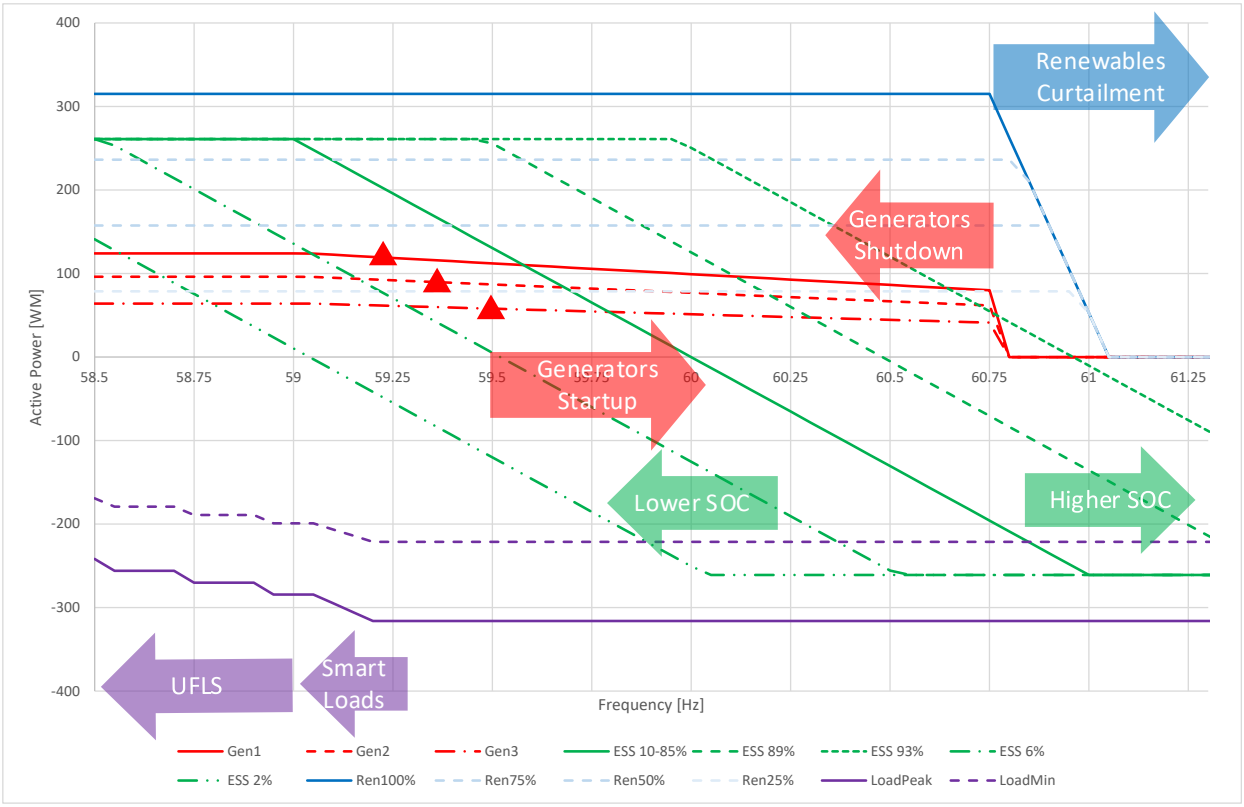

Figure 25. Communication-less frequency droop scheme. Values shown are for test run #7 with 100% renewables penetration and 82% ESS capacity.

We demonstrated the robustness of this method by operating the system across the following cases (shown in Table 1): the combined BESS power and energy ranged from 40 MW/120 MWh to 461 MW/4,665 MWh, and renewable penetration ranged from 20% to 300%. In the figure, the ESS duration corresponds to the size of each circle. Also, the color of the circle corresponds to actual renewables penetration measured as:

$$Measured\ Ren.Penetration\ [\%] = \frac{Ren.Energy\ [MWh]}{Ren.Energy\ [MWh] + Generators\ Energy[h]}$$

Table 1. Summary of all Cases Run with 9-bus Models.

Case No.	Duration	Renewable Penetration (%)	ESS Penetration (%)	ESS Duration (hours)	Inverters Enabled	Measured Ren. Pen.
1	1 day	20	12.7	0.88	3	8
2	1 day	20	12.7	0.38	3	8
3	1 day	50	45.71	3.36	5	20
4	1 day	50	82.86	6.87	7	20
5	1 day	100	45.71	3.36	5	41

Case No.	Duration	Renewable Penetration (%)	ESS Penetration (%)	ESS Duration (hours)	Inverters Enabled	Measured Ren. Pen.
6	1 day	100	82.86	6.87	7	41
7	1 day	100	146.3	14.8	9	41
8	1 day	200	62.22	6.66	6	62
9	1 day	200	82.86	6.87	7	70
10	1 day	200	146.3	14.8	9	89
11	1 day	300	62.22	6.66	6	73
12	1 day	300	146.3	14.8	9	92
1	1 week	20	12.7	0.889	3	8
3	1 week	50	45.71	3.365	5	19
4	1 week	50	82.86	6.873	7	19
5	1 week	100	45.71	3.365	5	37
6	1 week	100	82.86	6.873	7	37
7	1 week	100	146.3	14.81	9	39
8	1 week	200	62.22	6.667	6	64
9	1 week	200	82.86	6.873	7	66
10	1 week	200	146.3	14.81	9	70
11	1 week	300	62.22	6.664	6	73
12	1 week	300	146.3	14.8	9	86
Flatirons Campus operation – real data						
NA	3 days	386	200	2.0	1	80

We simulated all 12 cases with 24-times acceleration such that one simulated day was equivalent to one real hour. The BESS SOC was reset to 80% after each case was run. The simulations were run in order of increasing renewable energy penetration and ESS penetration. Results for all BESS power outputs and frequencies, as well as total generation, are shown in Figure 26.

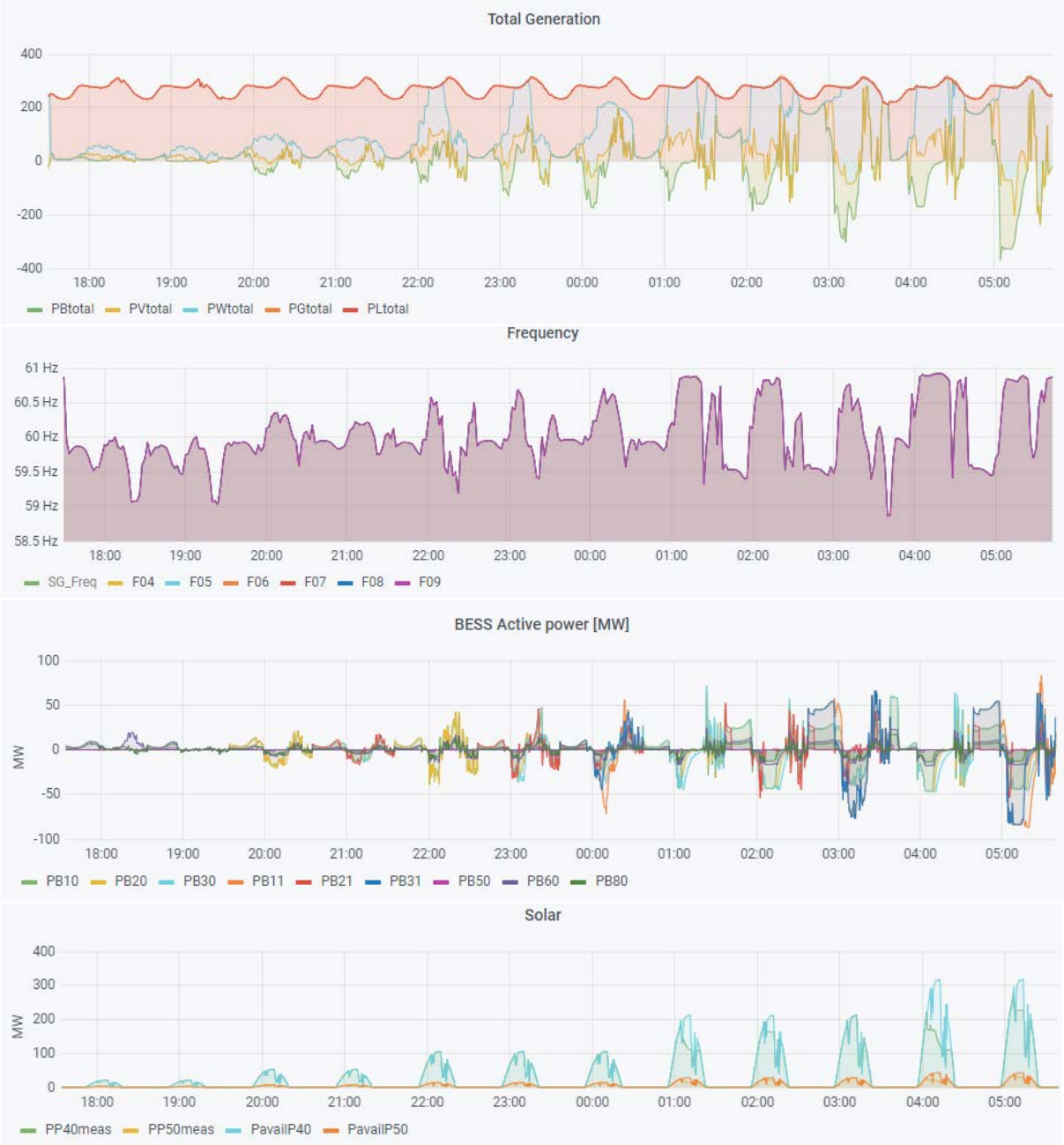

Figure 26. BESS power output and frequency, and total system generation, for all 12 simulated BESS rating and renewable power penetration scenarios.

As demonstrated in these simulation results, by allowing the system frequency to deviate from 60 Hz, the 9-bus system operates continuously with no blackouts in all scenarios simulated. We found that, in some cases, generators remained online for the entire simulation. In other cases, we slowly shut down the generators and were able to achieve near 100% renewable operation for an entire simulation day. The frequency in the system was maintained within the designed range of 59 Hz to 61 Hz. The only exception was at the beginning of Case 11 when generators had not properly started at the beginning of the experiments, most probably because of a delay in resynchronization during case initialization.

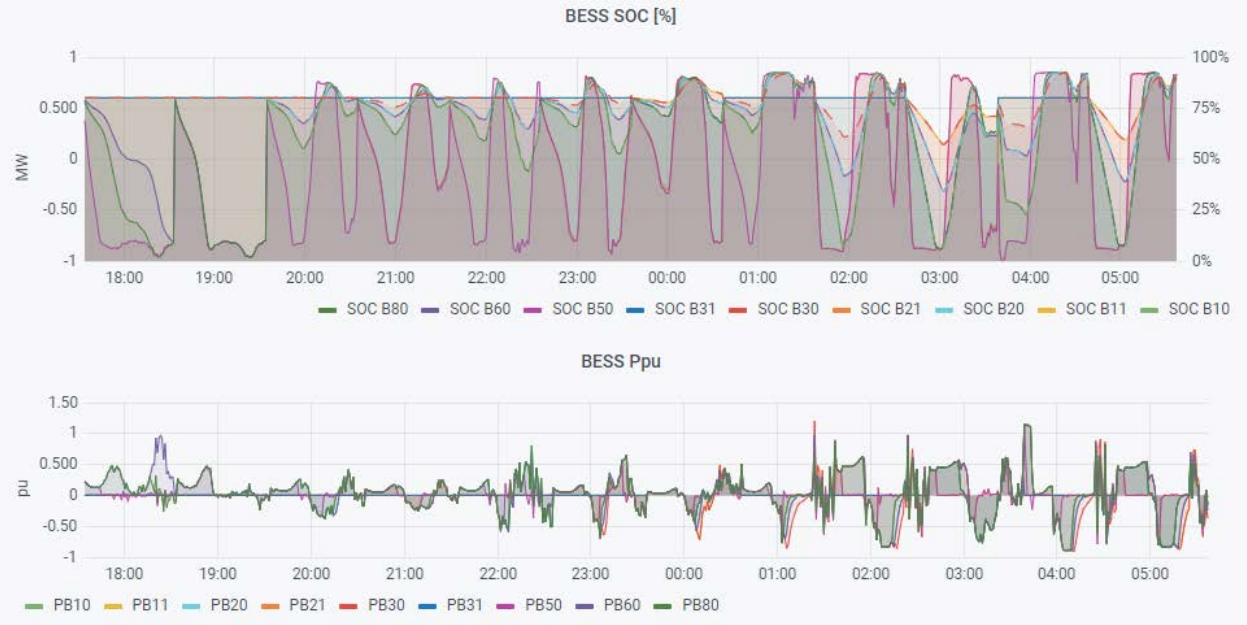

Figure 27. 9-times ESS operation data during 12 cases simulation.

Figure 27 shows operational data of the BESS during all cases. It shows that the SOC of all battery systems was maintained between 6% and 93% as long as the frequency was in the designed range. At the beginning of Case 11, one ESS nearly reached 0% SOC due to a prolonged below-nominal frequency. This indicates that certain protections and droop scheme enhancements can be made to prevent that from happening. The lower plot on the same figure shows per-unit power on each BESS. It is observed that the BESS are staying below +-1 pu range, except for two cases:

1. At the beginning of Case 11, when frequency was outside the nominal range for a prolonged period
2. At the end of Case 9, where a large amount of renewables dropped nearly at the same time. This required a lot of power to be drawn from the batteries, which, at the same time, were at a high SOC and allowed active power to exceed 130% of their ratings.

Both of these cases should be taken into consideration during development of further generations of grid-forming inverter models that should be able to limit their power to +-1 pu independent from grid frequency.

Another simulation using the 9-bus system was performed for a longer, seven-day stimuli vector shown in Figure 28. It was executed using 24-times the time acceleration—thus, the overall RTDS experiment took 7 hours. As opposed to the results shown before, this simulation shows a different operation of the system depending on the availability of renewable resources through multiple days. Configuration of this simulation was corresponding to Case 6, as described in Table 1, with 100% renewable penetration, 7 ESS inverters enabled with 82% capacity and overall duration of nearly 7 hours. The plot shows a generation mix during this experiment.

During Day 1, increased renewable production and high SOC of the BESS allowed two generators to be put offline—then restarted when PV production ramped down. The next two

days did not provide enough renewable power to fully recharge the batteries; therefore, the frequency was rather low and didn't allow the generators to disable. The situation changed on Days 4 and 5, when availability to renewable production allowed the ESS to be recharged. Two generators were shut down on Day 4 and a third went offline on Day 5—the system operated on 100% renewables for most of this day.

A sudden drop in wind production forced all generators to gradually come back online on Days 6 and 7. Because renewable capacity was relatively low at 100%, no renewable power curtailment was needed, and all renewable power produced either directly fed loads or was stored for future use—achieving optimal measured renewable penetration of 37%, as indicated in Table 1. Frequency never dropped below 59.2 Hz, so the system didn't require any support from smart loads or UFLS.

The communication-less scheme is able to handle operation of the ESS with different power (5 MW–100 MW) and duration ratings (1 hour–20 hours). The SOC of batteries with the same duration but different power ratings was nearly identical during the test period, while the SOC of the system with different durations, even when power ratings were different, was largely different. Fast ESS tend to quickly go through their capacity when needed, are cycled more often, and are typically saturated near the low and top of the SOC range. Large batteries are typically last to reach saturation. These results show that integrating various ESS technologies (e.g., Li-ion, hydrogen, pumped hydro, or even fast flywheel and super capacitors) is possible.

Another seven-day run was performed using the same profiles, but with much higher renewable penetration (300%) and ESS penetration (146%) at nearly 15 hours of storage duration (Case 12). Results of this run are shown in Figure 29. As expected, the period of operation of the generators decreased drastically; they were only active overnight after Days 1, 2, 6, and 7. The system operated for three full days using only renewable power. The ESS rarely needed to discharge below 10%, so frequency was pretty high and no smart loads or UFLS were necessary. Because the renewables largely exceeded the ESS and loads capacity, renewables curtailment was needed and operated smoothly, as shown in Figure 30. Graphs in this figure show the available power on the wind and PV systems that had to be curtailed.

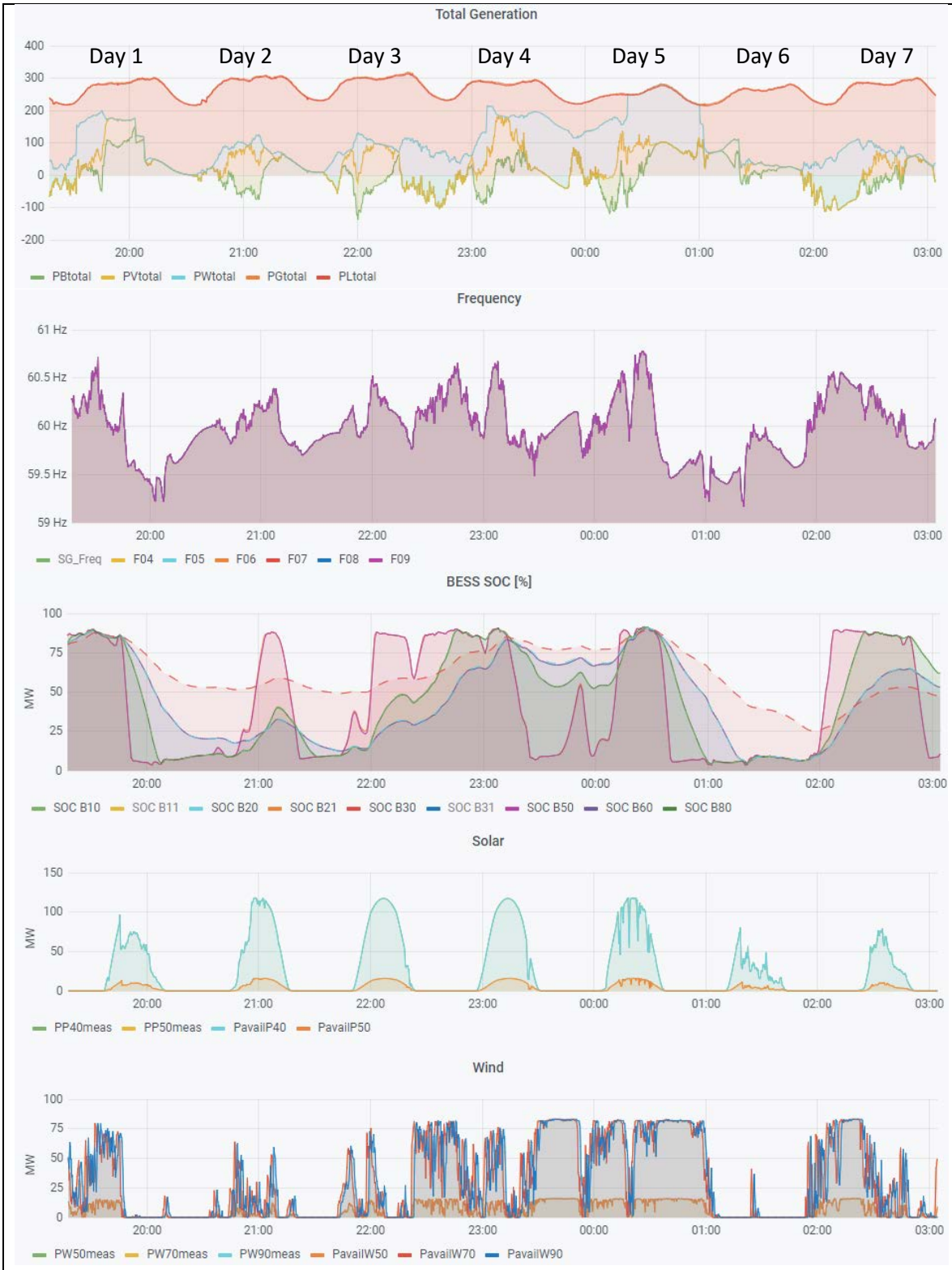

Figure 28. Case 6, run with a 7-day test profile, shows stable operation at 100% renewable penetration, 82% ESS penetration, and 7 hours ESS duration (7 out of 9 ESS inverters are active).

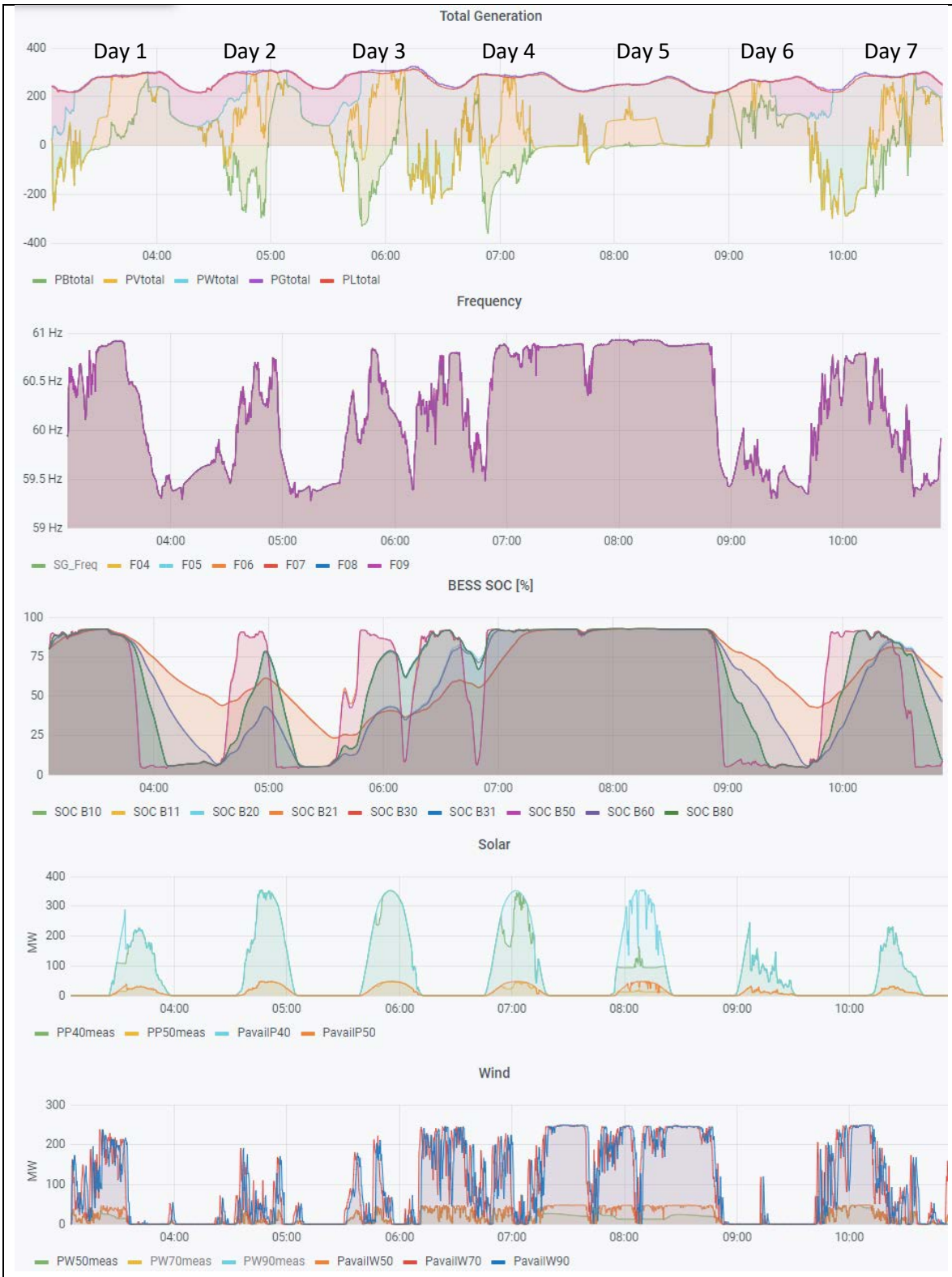

Figure 29. Case 12, run with a 7-day test profile, shows stable operation at 300% renewable penetration, 146% ESS penetration, and 15 hours ESS duration (all 9 ESS inverters are active).

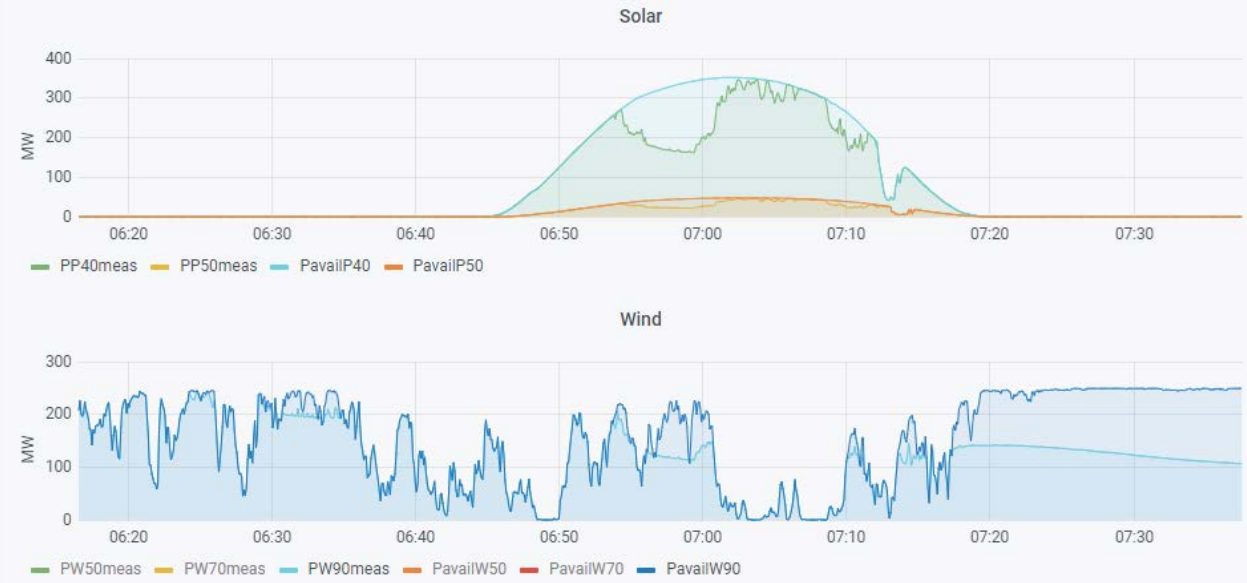

Figure 30. PV and wind curtailment during 7-day Case 12 simulation.

6.1 System Analysis Using a Simplified Grid Model

To analyze the frequency of the simulated scenarios, we developed a mathematical model in MATLAB that allowed precise frequency estimation for systems consisting of:

- Combined loads
- Combined renewable generation with droop
- A grid-forming battery (combined power and capacity of all batteries in the system)
- Three conventional generators with start/stop logic

This model is very fast because of sampling lowered to 1 minute, capable of a 7-day simulation in less than 1 second. The model also contains a 7-day test vector based on loads and real wind, and PV data from the Flatirons Campus site filtered similarly as described in the previous chapter (Figure 31). These data are typically available to power systems operators and could be used as inputs to the model to allow for planning a system transition from no-renewables and BESS systems to 100% renewables—as well as to tune the system with appropriate droop settings before it gets deployed.

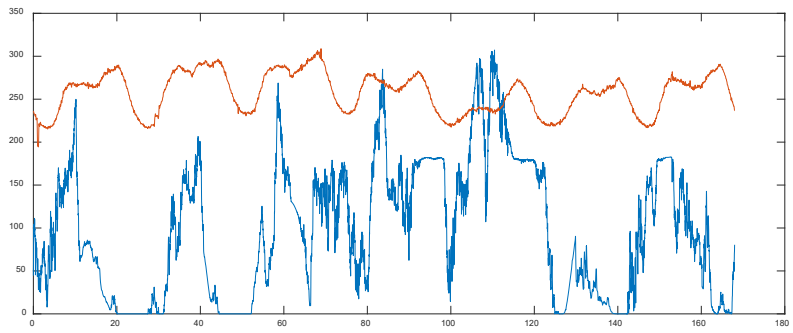

Figure 31. Seven-day, 1-minute resolution input data used for analysis. The orange line represents the combined load, the blue line represents combined renewables available power (PV and wind).

Because each simulation takes less than 1 second, thousands of simulations can be run to show performance of the system in various configurations of renewable power capacity and BESS capacity. Simulation results are summarized in Figure 32, showing how growth in renewables and BESS size affect generator contribution, renewable production and curtailment, and generator startup count.

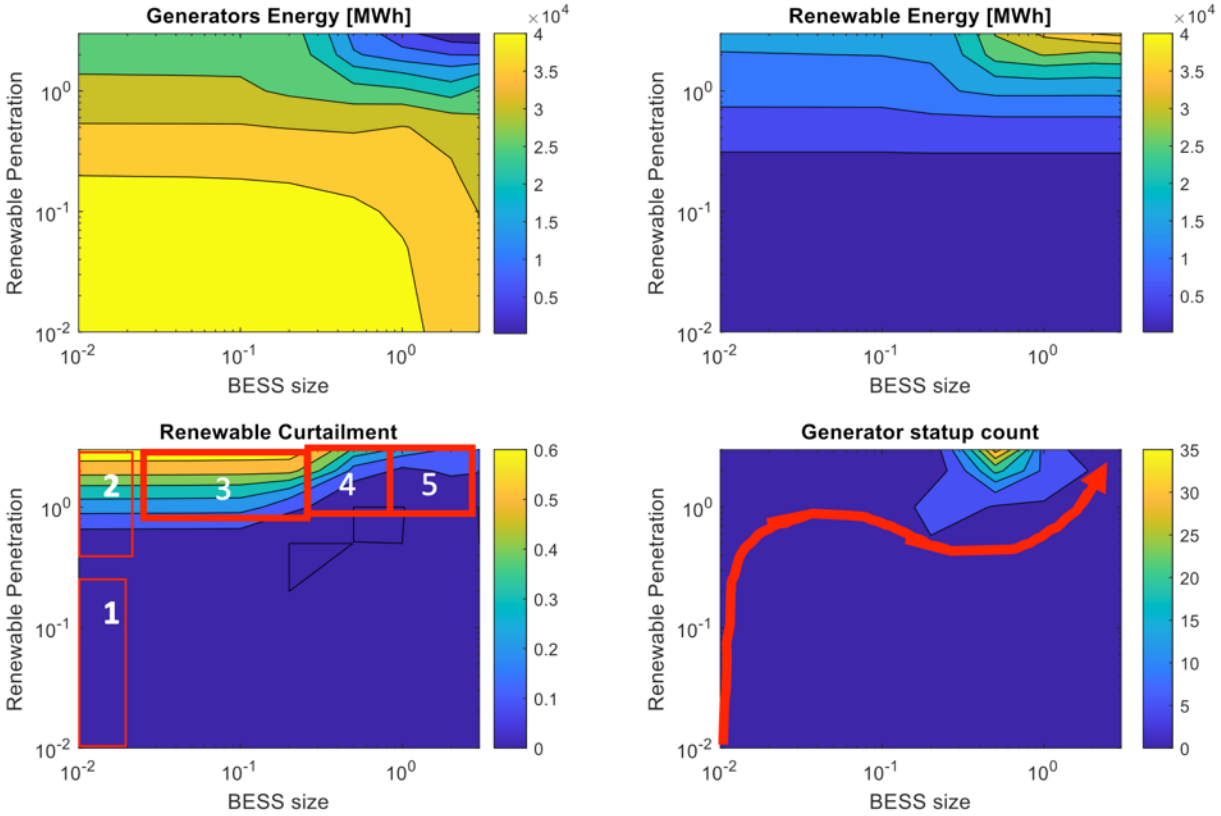

Figure 32. Results from thousands of simulations showing how higher levels of renewables and larger BESS systems impact conventional generation and renewable curtailment.

In the bottom-left graph in Figure 32, we show 5 phases that correspond to stages in renewable and BESS growth and illustrate unique impacts on curtailment and generator use. These phases are:

- Phase 1—corresponds to very little BESS capacity and increasing renewable penetration. Generally, no significant curtailment is visible up to 50% renewable penetration.
- Phase 2—corresponds to very little BESS capacity and relatively high renewable penetration levels, which requires higher curtailment. Our proposed communication-less method provides inherent renewable curtailment, as shown in previous sections, as well as in Figure 33, where a large amount of renewable capacity is installed with close to no BESS capacity, forcing large amounts of renewable power curtailment.
- Phase 3—corresponds to high renewable penetration and increased BESS capacity. The higher BESS levels enable the system to reduce energy from conventional generators. An example test run is shown in Figure 34, where the capacity of the BESS matched the capacity of PV in the system. This allowed for prolonged 100% renewable operation with no generator enabled, but still required a generator's participation at times when renewable generation was not consistent.
- Phase 4—corresponds to a combination of high renewable penetration and limited BESS, which causes generators to start and stop multiple times throughout the day. These results demonstrate that operators should avoid this scenario or implement smarter generator start-stop scheduling, including day-ahead forecasting or manual generator start-stop decisions.
- Phase 5—corresponds to sufficient BESS to enable a 100%-renewable grid using the control method proposed in this report. In this case, the generators could remain as backup in cases of unusual wind and solar resource conditions. An example run is shown in Figure 35, where the system is 100% renewable for an entire seven-day period.

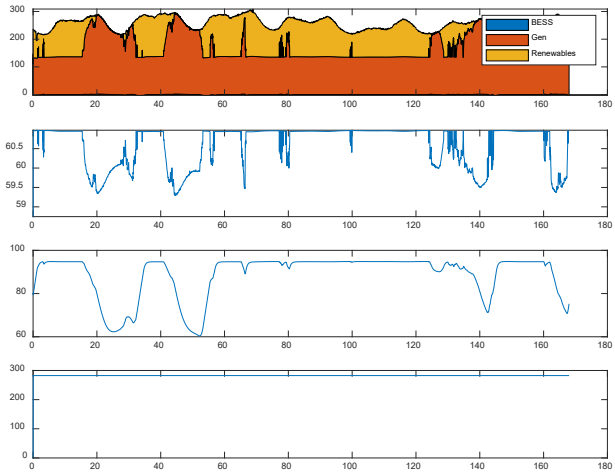

Figure 33. Example simulation result for system including 100% renewables capacity and close to 0% BESS capacity.

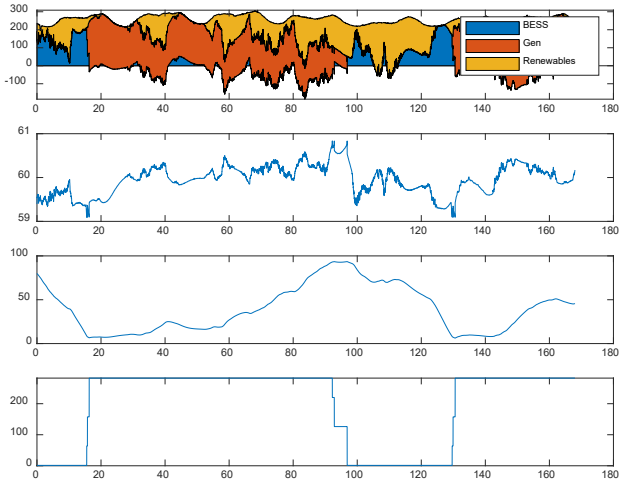

Figure 34. Example simulation result for system including 100% renewables capacity and 100% BESS capacity.

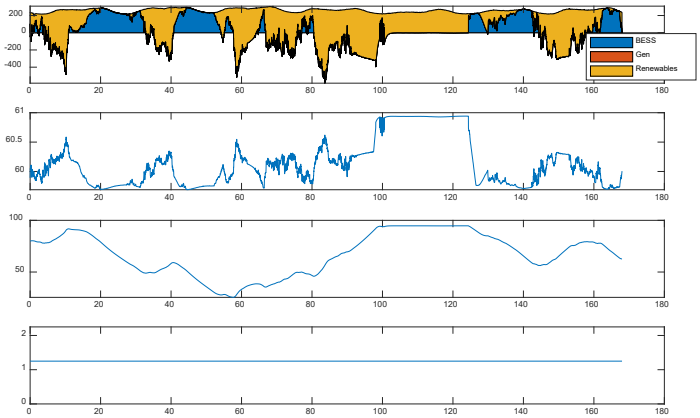

Figure 35. Example simulation result for system including 300% renewables capacity and 300% BESS capacity.

7 Limitations to the Proposed Control Method

There are several practical and technical limitations to deploying the proposed communication-less method, both on microgrids and larger grid systems.

Practically, integrating our proposed method encounters the usual challenges of deploying technologies in a multistakeholder power system. Particularly, different area operators and their diverse operational constraints would complicate power exchange between areas. Despite the simplicity that the communication-less method confers to renewable integration, deploying these resources across operator boundaries would require a more standardized treatment of the method. Also, transmission-line constraints could impact the viability of this method for wide-scale power exchange.

Furthermore, this method presumes an entirely different market environment for energy resources. For this method to be functional, system operators will need to modernize their tools for calculating economic dispatch and scheduling resources. Such modern tools will have the capability to value the variability of resources and assess their impact on system reliability. As more systems trend to higher levels of renewables and BESS, such tools will become more important and will facilitate a communication-less, plug-and-play scheme as presented here.

Technically, one challenge of the proposed method is the tendency for analog clocks to desynchronize. As a result, communication-less systems do not have a reliable reference on which to base their frequency analysis. There are several proposed strategies to overcoming this challenge, including analog clock correction and GPS-coordinated internal clocks.

Another technical challenge relates to grid-forming inverter technology and the standardization in deploying these controls on diverse commercial hardware. Currently, the technical landscape is relatively unconstrained and numerous vendors are producing non standardized inverter models capable of grid-forming controls, which would require that each product implement a custom set of controls. However, recent initiatives are focused on streamlining and standardizing grid-forming inverter designs.

8 Considerations for Implementation

This method could be applied at a variety of scales and for different purposes. Users hoping to implement this method should consider a few details that depend marginally upon the intended use.

First, simple as this strategy is, it is still within the technically challenging domain of power systems. NREL was able to deploy the method off the cuff because we work with the assets every day and are trained in low-level aspects of their operation. The guidance we provide in this report is sufficient to configure the same microgrid, given familiarity with power system assets like inverters and generators, and principles like droop, protection, frequency, and electrical safety of inverters and generators.

Such familiarity would be commonplace within a utility but might be absent at the scale of a neighborhood, building, or home. To apply our method without technical proficiency, we propose that devices come preconfigured with an option for communication-less/failsafe operation, using this approach. Users can then simply select the mode when needed—a very useful option in the wake of a disaster, when energy resources may be scraped together by individuals unfamiliar with power systems. Alternatively, we believe that the method could be conveyed in a simplified way that allows a non-specialist to understand and configure the device settings themselves.

The range in user specialty could also dictate the complexity of deployment. For example, the most bare-bones failsafe settings would be truly plug and play—the ranges for frequency and SOC are set, requiring no further attention. However, a utility or microgrid operator may want to integrate the failsafe mode with secondary controls or deploy the method across many distinct microgrids. For this, users could perform a similar system analysis as described in Sections 6.1 and 5.2; the authors may formalize and release this analysis code in the future. With deeper knowledge of system dynamics, specialist operators could then layer our method with controls that optimize for energy from renewables, or another operational target.

To ease deployment across different applications and scales, the authors propose that a certification or standard be developed for "communication-less, failsafe operation." Such a certification could streamline system configuration; for example, the military could certify its microgrid assets to have a guaranteed, core functionality for a wide range of deployment sizes, locations, and technology types.

Another consideration is the technical requirements of this method. Specifically, the battery inverter or other energy storage system should have adequate grid-forming capacity. This not only relates to the controls (SOC-based control and frequency droop are quite generic functionality), but also the power capacity of the assets. NREL used a BESS inverter that is 2.2-times greater than the rated BESS system power, which provides grid-forming functions like temporary overcurrent (useful for black starts and faults protection coordination (Gurule et al. 2019)) and voltage and frequency stability, as units connect and disconnect from the microgrid.

Protection and grounding are essential safety considerations and are active areas of research in the domain of grid-forming inverters. This report did not describe the protection scheme used by

NREL which utilized multiple research-specific medium- and low-voltage protective relays and breakers, and inverters' internal protection functions. Thanks to oversizing the BESS inverter, the short circuit power available allowed using standard protections typically seen in medium- and low-voltage distribution systems.

Lastly, we point out that there are more energy devices than just wind turbines, PV, diesel gensets, and battery storage. Applying our method on assets beyond the approach explained in this report will require consideration of those devices' droop and dynamic characteristics but in principle the droop method is agnostic of resource type.

9 Summary and Possible Applications of the Method

The proposed method is an uncomplicated solution to integrate higher levels of renewables and BESS with conventional generation—or operate with 100% renewables. This solution is scalable, requiring no changes to the underlying controls for larger-scale deployments, and plug-and-play, allowing generally any renewable asset to be simply interconnected without readjusting system parameters or a central controller. Being communication-less, it is also a useful method for improving cybersecurity and system resilience. The former because the number of data connections between energy resources is effectively reduced by 99%, cutting possible entries for bad actors; the latter because any variety of resources can be quickly combined to provide a resilient microgrid for disaster recovery or remote operation. The proposed method can be used in quick recovery of emergency power supply of segments of distribution systems followed by long-term outages caused by natural disasters of substation equipment failures. Grid-forming BESS can safely black start and operate an islanded grid, including distributed PV and local loads, without deploying a central controller for extended periods of time while a recovery process is underway. This can become a useful solution for U.S. island territories—such as Puerto Rico and the U.S. Virgin Islands—that are periodically prone to massive power outages because of hurricanes.

This paper described how our communication-less control method is functional for both a microgrid campus and a community-sized system. The microgrid demonstration of our method occurred unexpectedly; therefore, it also served as an example of system recovery and resilience. Because of the urgency around restoring power to NREL's Flatirons Campus (with more than 180 full-time staff), we developed a control solution that could be expediently deployed without significant oversight or customization. This also demonstrated an alternative to centralized controllers, which could save grid operators from possible large investments.

On the larger system simulation, representing a 315-MW system, we showed that our communication-less method created interesting dynamics in curtailment and conventional generator operation. Specifically, as a similarly sized system increases its proportion of renewables and BESS, bulk generators more often switch between on and off at a certain high proportion of BESS and renewables. This finding could help system operators begin to plan how to best implement such a method for economic savings and renewable deployment.

Following the success of this method on a real campus and on a simulated community system, there are research opportunities to expand the method to larger systems, such as the Hawaiian Islands, where high renewable systems are currently pushing full renewable operation. Future

demonstrations could also consider hybrid approaches in which some assets are communicating to central grid controllers to optimize operation. For example, only utility-scale systems greater than 20 MW could communicate with a central coordinator while all smaller assets could operate solely off frequency. In this case, aggregators of DERs would not be necessary because the energy resources would not require individual management or coordination.

Analyses performed so far don't touch on economic and optimization aspects of the communication-less method and will require further study.

Our results demonstrate that a communication-less, frequency-based method for managing DERs is feasible at multiple scales. In practice, this method could provide a path to transition to 100% renewable power because it provides a straightforward approach for integrating renewables with conventional generation at any proportion. It could also support resilience, stability, and economics of grid operation. Our group plans to continue this research focus to further validate communication-less methods at scale.

References

NERC. 2017. *Distributed Energy Resources: Connection Modeling and Reliability Considerations*. NERC. www.nerc.com/comm/other/essntlrlbltysrvcstskfrcdl/distributed_energy_resources_report.pdf

Lin, Yashen, Joseph H. Eto, Brian B. Johnson, Jack D. Flicker, Robert H. Lasseter, Hugo N. Villegas Pico, Gab-Su Seo, Brian J. Pierre, and Abraham Ellis. 2020. *Research Roadmap on Grid-Forming Inverters*. Golden, CO: National Renewable Energy Laboratory. NREL/TP-5D00-73476. https://www.nrel.gov/docs/fy21osti/73476.pdf.

High Share of Inverter-Based Generation Task Force. 2022. *Grid-Forming Technology in Energy Systems Integration*. Reston, VA: Energy Systems Integration Group. https://www.esig.energy/reports-briefs.

Eto, J. H., Robert Lasseter, David Klapp, Amrit Khalsa, Ben Schenkman, Mahesh Illindala, Surya Baktiono. 2018. *The CERTS Microgrid Concept, as Demonstrated at the CERTS/AEP Microgrid Test Bed*. Lawrence Berkeley National Laboratory. https://eta-publications.lbl.gov/sites/default/files/certs_microgrid_concept_final.pdf

Abrahamsen, F. E., Yun Ai, Michael Cheffena. 2021. *Communication Technologies for Smart Grid: A Comprehensive Survey*. https://www.mdpi.com/1424-8220/21/23/8087

DOE. 2015. *An Assessment of Energy Technologies and Research Opportunities*. DOE. https://www.energy.gov/sites/prod/files/2015/09/f26/Quadrennial-Technology-Review-2015_0.pdf

Johnson, J., Ifeoma Onunkwo, Patricia Cordeiro, Brian J. Wright, Nicholas Jacobs, Christine Lai. 2020. *Assessing DER network cybersecurity defences in a power-communication co-simulation environment*. IET Cyber-Physical Systems: Theory & Applications. https://ietresearch.onlinelibrary.wiley.com/doi/full/10.1049/iet-cps.2019.0084

A. Huque, E. F. 2021. *Grid-Forming Inverters: EPRI Tutorial*. EPRI. https://www.epri.com/research/products/000000003002018676